SYNTHESIS AND CHARACTERIZATION OF PLATINUM BASED CATALYSTS FOR FUEL CELLS

by

SONAM PATEL

Presented to the Faculty of the Graduate School of

The University of Texas at Arlington in Partial Fulfillment

of the Requirements

for the Degree of

MASTER OF SCIENCE IN MATERIALS SCIENCE AND ENGINEERING

THE UNIVERSITY OF TEXAS AT ARLINGTON

MAY 2011

ACKNOWLEDGEMENTS

I would like to express my gratitude to Dr. Efstathios Meletis and Dr. Yaowu Hao for their support and patience in reviewing my thesis and being a part of the defense committee. I would also like to show my appreciation towards all the professors in the Department of Materials Science and Engineering for offering their knowledge and guidance. I'd like to thank the administrative secretaries Jennifer Standlee and Libia Cuauhtli, for their contribution in my academic paper works.

I'm truly grateful to my advisor, Dr. Fuqiang Liu, for giving me his valuable supervision and expertise and for always taking the time out to guide me during every stage of this thesis, without which this thesis would not have been possible. It is also my pleasure to thank Dr. Jiechao Jiang, David and the entire staff of Center for Characterization and Materials (CCMB) lab for training me on various facilities and assisting me in using their equipment at all times.

I'd also like to extend my sincere gratitude to all the lab members: Md Noor e Alam Siddique, for helping me and providing his guidance and time in using TEM and HR-TEM, Dong Liu for always being there to provide me with his expertise in the lab, Chia Jen Hsu and Syed D Sajjad for sharing their knowledge. The animated atmosphere created by all the group members has truly made this a memorable and enjoyable place to work in.

Last but not the least I'd like to extend my heartfelt appreciation to all my friends for their support and above all my parents for always encouraging and motivating me throughout my life.

April 15, 2011

ABSTRACT

SYNTHESIS AND CHARACTERIZATION OF PLATINUM BASED CATALYSTS FOR FUEL CELLS

Sonam Patel, M.S.

The University of Texas at Arlington, 2011

Supervising Professor: Fuqiang Liu

Platinum (Pt) and platinum alloys have attracted wide attention as catalysts to attain high performance to increase the power density and reduce the component cost of polymer electrolyte membrane fuel cells (PEMFCs). Extensive research has been conducted in the areas of new alloy development and understanding of mechanisms of electrochemical oxygen reduction reaction (ORR). The durability of PEMFCs is also a major barrier to the commercialization of these fuel cells. Recent studies have suggested that potential cycling can gradually lead to loss of active surface area due to Pt dissolution and nanoparticle grain growth [1].

In this thesis we report a one-step synthesis of highly-dispersed Pt nanoparticles and Pt-Cobalt supported on Ketjen carbon black (20% Pt/C & 20% Pt_3Co/C) as electro-catalysts for PEMFCs. Pt particles with size in the range of ~ 2.6nm (Pt/C) and 3.9 nm (Pt_3Co/C) were

obtained through adsorption on carbon supports and subsequently thermal decomposition of platinum acetylacetonate ($Pt(acac)_2$). A comparative characterization analysis, including X-ray diffraction (XRD), high resolution transmission electron microscope (HR-TEM), FT-iR, EDAX, cyclic voltammetry (CV), and oxygen reduction reaction (ORR) activity, was performed on the synthesized and commercial (46.5wt% TKK) catalysts. The analysis was to reveal the Pt dispersion on the carbon support, particle size and distribution, electrochemical surface area (ECA), and ORR activities of these catalysts. It was found that the synthesized Pt/C showed similar particle size to that of the TKK catalysts (2.6nm and 2.7nm, respectively), but narrower particle size distribution; while the particle size for Pt_3Co/C was found to be ~3.9 nm. Accelerated durability tests (ADT) under potential cycles were also performed for Pt/C and TKK to study the electrochemical degradation of the catalysts in corrosive environments. The ADTs revealed that the two catalysts (Pt/C & TKK) were comparable with respect to degradation in ECA and ORR activities. Initial electrochemical evaluation of Pt_3Co/C was conducted, but durability studies were not attempted in this thesis due to its worse ORR kinetics than those of the Pt/C catalyst. From the experimental data, it was found that particle size impacted negatively the ECA and ORR activity of the catalysts.

TABLE OF CONTENTS

LIST OF ILLUSTRATIONS

LIST OF TABLES

Table Page

CHAPTER 1

INTRODUCTION AND OBJECTIVES

Polymer electrolyte membrane fuel cells (PEMFCs) are among the most viable candidates for next generation, clean, and potentially fossil fuels independent electric vehicles. They offer broad advantages over conventional heat engines. Mechanical Heat Engines use the heat released by the reaction of a chemical substance (fuel) with oxygen (usually from the air). This heat is then converted to mechanical energy by means of complex machinery, and the whole process is cumbersome and inefficient. Rather, converting chemical energy directly into electricity is a more straight forward method, considering the electric nature of the chemical bonds that hold the atoms in a molecule.

Devices that can convert chemical energy directly into electrical energy are called electrochemical cells [2]. Since electrochemical cells convert chemical energy directly into electrical energy without the intermediate degradation into heat, they are not limited by the Carnot efficiency. Electrochemical cells are categorized broadly as expendable or nonexpendable; the former cannot be preserved after its first discharge, while the latter is considered as reusable. And the nonexpendable cells can be further subcategorized as either rechargeable, i.e., their activity can be restored by means of an electric charging current, or refuelable (fuel cells), which deliver a sustained output as their consumables are replenished [2].

Fuel cells can be classified mainly by the kind of electrolyte used. This classification determines the kind of chemical reactions that take place in the cell, the kind of catalysts required, the temperature range in which the cell operates, the fuel required etc. These characteristics, in turn, affect the applications for which these cells are most suitable. There are several types of fuel cells currently under development,

each with its own advantages, limitations, and potential applications. The following chart is a comparison of fuel cell technologies according to [3].

Table 1.1 Comparison of Fuel Cell Technologies Chart, [3]

Fuel Cell Type	Common Electrolyte	Operating Temperature	Typical Stack Size	Efficiency	Applications	Advantages	Disadvantages
Polymer Electrolyte Membrane (PEM)	Perfluoro sulfonic acid	50-100°C 122-212° typically 80°C	< 1kW-100kW	60% transpor-tation 35% stationary	• Backup power • Portable power • Distributed generation • Transporation • Specialty vehicles	• Solid electrolyte re-duces corrosion & electrolyte management problems • Low temperature • Quick start-up	• Expensive catalysts • Sensitive to fuel impurities • Low temperature waste heat
Alkaline (AFC)	Aqueous solution of potassium hydroxide soaked in a matrix	90-100°C 194-212°F	10-100 kW	60%	• Military • Space	• Cathode reaction faster in alkaline electrolyte, leads to high performance • Low cost components	• Sensitive to CO_2 in fuel and air • Electrolyte management
Phosphoric Acid (PAFC)	Phosphoric acid soaked in a matrix	150-200°C 302-392°F	400 kW 100 kW module	40%	• Distributed generation	• Higher temperature enables CHP • Increased tolerance to fuel impurities	• Pt catalyst • Long start up time • Low current and power
Molten Carbonate (MCFC)	Solution of lithium, sodium, and/ or potassium carbonates, soaked in a matrix	600-700°C 1112-1292°F	300 kW-3 MW 300 kW module	45-50%	• Electric utility • Distributed generation	• High efficiency • Fuel flexibility • Can use a variety of catalysts • Suitable for CHP	• High temperature cor-rosion and breakdown of cell components • Long start up time • Low power density
Solid Oxide (SOFC)	Yttria stabi-lized zirconia	700-1000°C 1202-1832°F	1 kW-2 MW	60%	• Auxiliary power • Electric utility • Distributed generation	• High efficiency • Fuel flexibility • Can use a variety of catalysts • Solid electrolyte • Suitable for CHP & CHHP • Hybrid/GT cycle	• High temperature cor-rosion and breakdown of cell components • High temperature opera-tion requires long start up time and limits

From the above listed types of fuel cells, the PEMFC or solid polymer electrolyte fuel fells (SPFCs) offer the advantages of low weight and volume, as the electrolyte is a solid membrane. It is theoretically the simplest of fuel cells and potentially the easiest to manufacture. Also PEMFCs operate at relatively low temperatures, around 80℃ (176℉) [3]. **Due to their low operating temperatures, the kinetics of PEMFCs are unacceptable unless special catalysts are used.** These catalysts therefore include noble metals (platinum based) which have therefore made the cost of these fuel cells inhibitive.

Certain approaches have been made in the past to reduce the cost of the hydrogen PEMFCs, mainly focusing on the catalyst materials, such as

- Reducing the platinum loading (in mg_{Pt}/cm^2 on a geometric basis of a electrode) while making the catalysts more active
- Reducing the particle size, based on the fact that when reducing the grain size, the surface to volume ratio is increased, i.e., less platinum is needed for a given platinum area.
- Alloying platinum with cobalt and other transitional metals, in an attempt to reduce the amount of platinum used as well as to make the catalyst more active toward ORR.

Objectives:

The objective of this thesis was to study a simple method that would potentially provide high-activity and high-durability fuel cell catalysts, which also eventually bring down the cost since the processing cost has been a major impediment to synthesizing fuel cell catalysts.

The state-of-the-art Pt-based catalysts supported on carbon are routinely prepared through tedious wet-chemistry steps, including filtering, pH control, cleaning/washing, and drying. Moreover, the ability to control particle size, composition, as well as to achieve element mixing between Pt and the transitional metals remains elusive in wet-chemistry approaches. In this thesis, a one-step synthesis of highly dispersed fuel cell catalysts has been explored. The catalyst properties depend on a strong interaction between the Pt precursors (Platinum acetylacetonate, $Pt(acac)_2$ as adsorbate) and substrate (Ketjen carbon black) surface. Both the oxygen reduction activity and electrochemical durability have been studied.

CHAPTER 2

LITERATURE SEARCH

2.1 Principle of PEMFC

Research activities on PEMFCs have gained a lot of momentum during the past decade [4]. However, the currently state-of-the-art fuel cell systems still need to be made economically acceptable with high performance and durability. It is essential to understand the relationship between the structure, properties, processing and performance in order to search for cost-effective materials [5].

2.1.1 Principle

A schematic of the cell configuration and basic operating principles is shown in Figure 2.1. A PEMFC contains a membrane electrode assembly (MEA) typically consisting of an ionic conducting polymer membrane which acts as the electrolyte [6], sandwiched between two electronically conducting electrodes [3]. At the interface between the porous electrode and the polymer membrane, exists a catalyst layer, typically made of platinum supported on carbon [6].

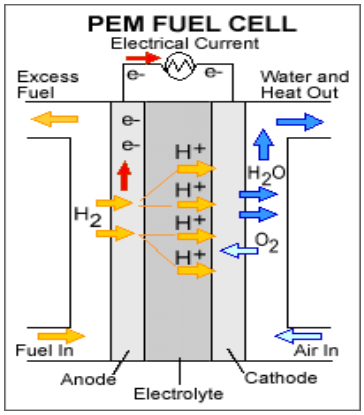

Figure 2.1 Schematic Diagram of the basic operating principle [6].

The electrochemical reactions occur at the surface of the catalyst [6] as the schematic configuration and basic operating principles in Figure 2.1 show. Hydrogen entering from the anode side of the cell splits into proton and electron; the proton permeates through the membrane which must exhibit ionic conductivity and the electron travels through the electrically conductive electrodes, current collectors, and the outside circuit where they perform useful work. At the cathode side, the electron generated at the anode along with the proton that permeates through the membrane and the oxygen entering from the cathode side combine to form water and heat.

The basic fuel cell reactions are:

$$\textbf{Anode: } 2H_2 \rightarrow 4H^+ + 4e^- \quad \textbf{(2.1)}$$

$$\textbf{Cathode: } O_2 + 4H^+ + 4e^- \rightarrow 2H_2O \quad \textbf{(2.2)}$$

$$\textbf{Overall: } 2H_2 + O_2 \rightarrow 2H_2O + \text{energy} \quad \textbf{(2.3)}$$

The net result of these simultaneous reactions is current of electrons through an external circuit, i.e., direct electrical current [6].

2.1.2 Fuel Cell Components and Properties

The PEMFC mainly comprises of four main components, namely

- Membrane
- Electrodes
- Gas Diffusion Layer
- Bipolar Plates

2.1.2.1 Membrane

The three main properties a fuel cell membrane must exhibit are protonic conductivity, a barrier to mixing of fuel and reactant gases, and chemical and mechanical stability within the fuel cell environment. Typically, the membranes for PEMFCs are made of perfluorocarbon-sulfonic acid ionomer (PSA). This is essentially a copolymer of tetrafluorethylene (TFE) and various perfluorosulfonate monomers. The best known is Nafion made by Dupont [6].

2.1.2.2 Electrodes

The challenge in the design of a PEMFC arises in designing the catalyst layer which is heterogeneous and complex. The catalyst and the catalyst layers are required to be designed so as to generate high rates of desired reactions and minimize the amount of catalysts for reaching the required levels of power output. In order to achieve this, a few requirements need to be considered such as to ensure large interfacial area between the polymer electrolyte and catalyst, efficient transport of protons across the membrane from the anode to cathode, easy transport of reactant gases and products, and continuous electron passage between the reaction spots and the massive current collector [2].

The electrode of a fuel cell is nothing but a thin layer of catalyst embedded between the ionomer membrane and a porous, electrically conductive substrate. It is also the layer where the electrochemical reactions take place [6]. Typical electrodes for PEMFC applications are made of a gas diffusion layer (usually porous carbon paper or carbon cloth) supporting a layer of finely dispersed platinum on carbon catalysts. The reaction zone can be amplified by either roughening the surface or by reducing the catalyst particle size or incorporating the ionomer in the catalyst layer [6]. Platinum is the most extensively used metal in the anode and cathode electrodes because of its high catalytic activity for both oxidation and reduction reactions [7]. However, **the high cost of Pt is prohibitive for commercial applications of PEMFCs** and research efforts are currently directed towards reduction in the amount of platinum utilized by improving MEA preparation techniques [8-12].

In order to achieve uniform and highly dispersed Pt loadings, the PEMFC cathode catalysts are usually supported on carbon supports with a high surface area above $75 m^2/g$. Some of the common supporting materials are carbon blacks with a high degree of graphitic character: Vulcan XC-72R, Black Pearls BP 2000, Ketjen Carbon Black, etc. The support material must provide a high electric conductivity, high and uniform catalyst dispersion, as well as good reactant gas access to the catalyst with good corrosion resistance [13].

2.1.2.3 Gas Diffusion Layer

Some of the properties a gas diffusion layer must exhibit are,

- Must be sufficiently porous to allow permeability to gases, water and products.
- Must by electrically and thermally conductive.
- Must be sufficiently rigid to support the MEA

The above properties are best met by carbon fiber paper or woven carbon fibers. They are mostly hydrophobic in order to avoid the flooding in their bulk [6].

2.1.2.4 Bipolar Plates

Some of the properties bipolar plates must exhibit are,

-They connect cells electrically in series, therefore they must be electrically conductive

-They must be impermeable to gases as they separate gases in adjacent layers

-They must provide structural support.

-They must be thermally conductive as they conduct heat from the active cells to the cooling cells.

So far, two families of materials have been used for PEMFCs in the construction of the bipolar plates, namely graphite-composite and metals [6].

2.2 Catalyst Synthesis Processes

The main factors preventing PEMFCs from wide-spread applications are high cost and undesirable degradation of Pt-based electrocatalysts. The state-of-the-art Pt catalysts supported on carbon (Pt/C) are routinely prepared through impregnation-reduction [14], microemulsion [15] and ion exchange [16]. Pt-alloy catalysts have been mainly synthesized by incorporation of alloy metals on the pre-formed Pt/C in colloidal sol [17], sol-gel [18], hydroxide/hydrous oxide [8], and via carbonyl complexes [19]. Recently, monodispersed PtNiFe ternary nanoparticles have been synthesized from molecular encapsulation via the aid of capping agents [20]. This method has been successfully demonstrated to render binary [21] and ternary compositions [22]. In all cases mentioned above, the preparation involves tedious wet-

chemistry steps, including filtering, pH control, cleaning/washing, and drying. While several supported Pt-based binary or ternary catalysts have been prepared by different methods, the ability to control particle size, composition, as well as to achieve element mixing between Pt and transitional metals still remain elusive.

Pt nanoparticles have been formed by vacuum processes on different supports as an attempt to simplify the synthesis by dry processes. However, it was found that the particle size distribution was broad (between 2~13 nm) and insensitive to the growth conditions [23, 24]. Dry processing can also be implemented without a surface, although low solubility of the vapor-phase precursors makes particle nucleation and growth challenging. To overcome the limitation of low solubility, Pt deposition has been performed in supercritical carbon dioxide (sc-CO_2) at high pressure [25]. Organometallic Pt precursors that are more commonly used in vapor phase deposition were used. Pt particle synthesis by sc-CO_2 is very similar to the conventional wet process (impregnation and reduction); however, there are fundamental differences in particle nucleation and growth process. In conventional wet process, the particle synthesis process is controlled by diffusion rate of Pt ions in the liquid phase; while in the sc-CO_2 the particles form through thermal decomposition of the adsorbed organometallic precursors on the support. Therefore, in the sc-CO_2 deposition the surface mobility of adsorbates, which is controlled by surface properties of the support, dominates the particle formation. Though Sc-CO_2 deposition is a flexible and promising process to synthesize fuel cell catalysts, the high pressure (e.g., up to 240 atm in [12] and 150 atm in [25]) required to achieve the super-critical conditions brings up the issues of safety and equipment cost.

2.3 Electrocatalytic Oxygen Reduction Reactions (ORR)

In a PEMFC, including direct methanol fuel cell (DMFC), ORR is the reaction occurring at the cathode. Usually, the ORR kinetics is sluggish. But in order to speed up the process to reach a practical usable level, a cathode ORR catalyst is required. At present, the Pt based materials are the most widely employed catalyst materials [26].

2.3.1 Electrochemical Oxygen Reduction Reaction and Catalyst Durability

The mechanism of the ORR processes is quite complex involving intermediates, primarily depending on the natures of the electrode material, catalyst and electrolyte. The reduction pathways bear unique significance depending on the applications. In fuel cell processes, the 4-electron direct pathway is highly preferred. [26].

ORR activity depends critically on the structure of Pt particles. ORR takes several steps as shown in the following diagram,

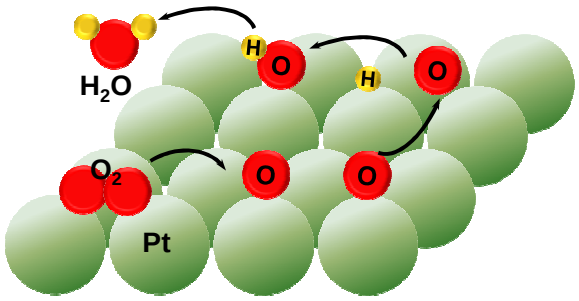

$$O_2 \rightarrow 2 *O \quad (*=\text{adsorbed}) \qquad (2.4)$$

$$*O + H^+ + e^- \rightarrow *OH \qquad (2.5)$$

$$*OH + H^+ + e^- \rightarrow H_2O \qquad (2.6)$$

Figure 2.2 Schematic diagram showing oxygen oxidation process on Pt surface.

During ORR, oxygen molecule splits into adsorbed oxygen atoms (equation (2.4)) and subsequently forms water (eqn. (2.6)). These reactions become the rate limiting steps in an ORR reaction. A match between O=O bond length (1.3Å) and Pt-Pt distance (~ 2.7 Å depending on composition and structure) plays an important role in oxygen dissociation at Pt surface. In order to enhance oxygen dissociative adsorption on the Pt surface, either Pt particle size needs be increased or Pt needs to be alloyed with base-metals. These methods can reduce the Pt-Pt distance and therefore promote further oxygen dissociative adsorption.

Although it is known that carbon supported platinum and its alloys have the best kinetics for oxygen reduction reaction [27], platinum has a small but finite solubility under highly acidic and oxidizing cathodic environment of PEMFCs. These catalysts can degrade through dissolution which is accelerated with

potential cycling. It has also been observed that Pt dissolution becomes more favorable for small particles due to high surface energy (Gibbs-Thomson effect). Pt dissolution can occur through the flowing process,

$$Pt \rightarrow Pt^{2+} + 2e^{-} \text{ (at 1.188V)} \quad (2.7)$$

where Pt atom is electrochemically oxidized to Pt^{2+} ion. Thermodynamically, this reaction (eqn. (2.7)) occurs at equilibrium potential of 1.188V, which, however, can be altered by bonding energy and coordination number of Pt at particle surface depending on structures.

2.3.2 Particle Size Effect

Both ORR activity and catalyst durability strongly depend on catalyst crystallographic structure. Several models have been put forward to draw correlations between the particle size and population of crystallographic surface sites associated with atoms at edges, kinks and vertices. Among these, Ramanowski [28] suggested the cubo-octahedran structure as a possible model. The model aimed at minimizing the surface energy. This basic model consists of eight (111) and six (100) crystal faces, bound by edge and corner sites associated with edge, kink and corner sites. In another review, Kinoshita used this model to correlate the surface-averaged distribution (Figure 2.3) of (111), (100) and edges and kinks, as a function of particle size. It was observed that the low-index surfaces and defects (including edges and kinks) decrease with increasing particle size [28].

The particle size thus would strongly affect catalyst durability, as Figure 2.4 demonstrates. It shows a shift in the onset of oxide adsorption/desorption for Pt polycrystalline by 80mV compared to TKK, while that for Pt black falls inbetween. This indicated that the large particles, with less surface defects, help to inhibit OH formation on Pt surface, enabling more fresh Pt surface available for reaction (therefore more active) [29].

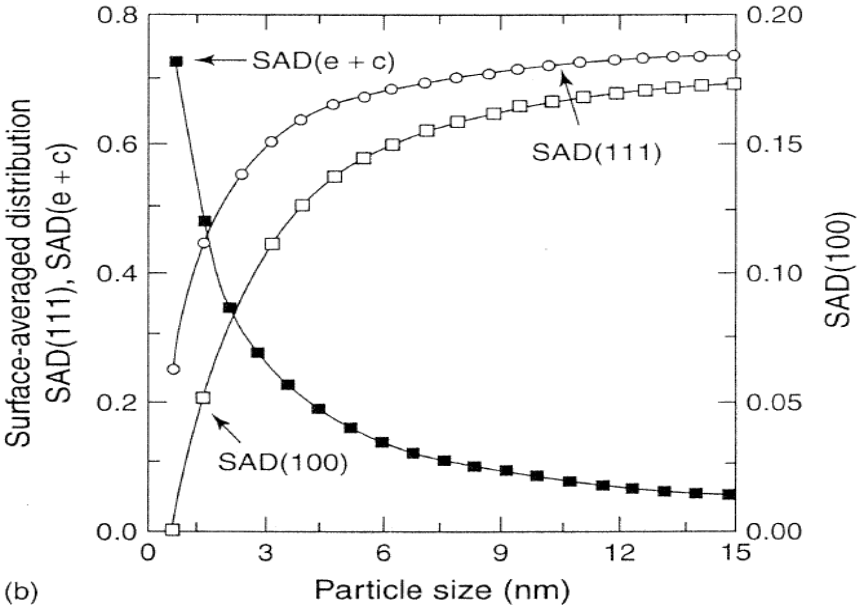

Figure 2.3 Particle size versus surface-averaged distribution [28].

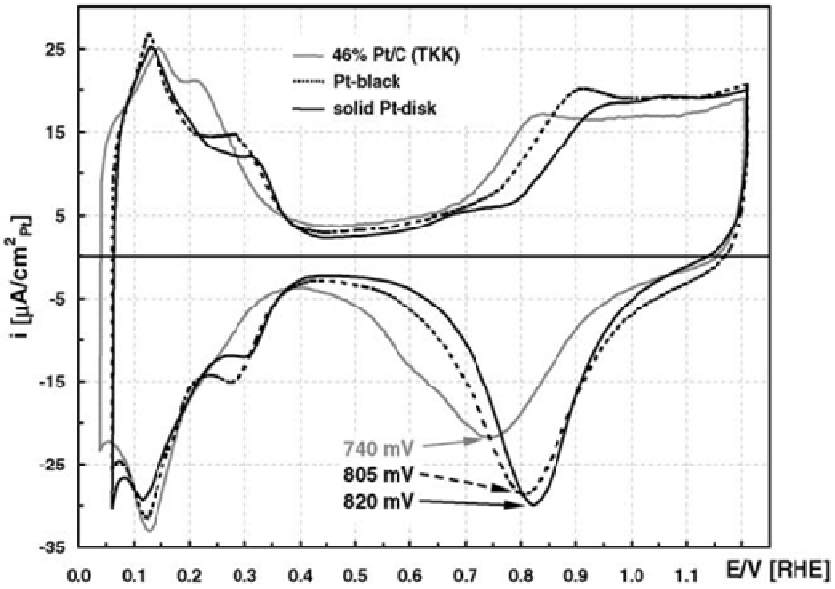

Figure 2.4 Cyclic voltammograms of carbon-supported Pt, Pt-black and 46% Pt/C(TKK) in terms of surface area [29].

2.3.3 Pt and Pt Alloy catalysts for PEM fuel cells

Currently, state-of-the-art MEAs are typically composed of highly dispersed Pt on carbon supports, often high weight % Pt on carbon support that ensures the formation of thin catalyst layers (Pt loading = 0.4mg/cm^2). The specific activity (i_s) of Pt supported on high-surface-area carbon at 80˚C under O_2 at a partial pressure of ~100kPa at 0.9V is about 180-210μA/cm$_{Pt}^2$ and the mass activity (i_m) is in the range of 0.11-0.16A/mg$_{Pt.}$ In order to meet the cost targets for commercialization of PEM fuel cells, it is essential to reduce the Pt-loading to ¼ of the current state-of-the-art MEA cathode catalyst layer, i.e., from 0.4 to 0.1mg/cm^2 without a loss in cell voltage, while maintaining maximum power density and cell efficiency. Also it is necessary to maintain the enhanced catalytic activity over ~5000h or more for automotive applications with low degradation rates of a few μV/h [29].

It was found that the main factor affecting the catalytic activity for oxygen reduction reaction other than particle size included alloying. Reducing the Pt-Pt nearest neighbor distance by alloying Pt with a transition element (e.g., Co, Fe, Ni) as Figure 2.5 shows, seemed to provide more favorable sites for the dissociative adsorption of oxygen. Studies have demonstrated that some base-metal elements with smaller atomic sizes than Pt, when alloyed with Pt, caused lattice contraction, while those base-metals with lattice expansion seemed to be less active [30]. The resultant decrease in the interatomic distance between Pt atoms has proven to increase the electro-catalytic activity for Pt alloys such as PtCr, PtV, PtTi, etc.

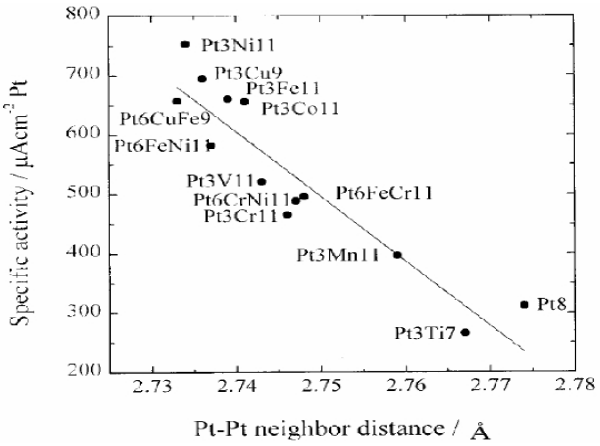

Figure 2.5 Relation between Pt-Pt nearest neighbor distance and specific activity [30].

Other strong correlations between the enhanced activity of Pt alloys, over Pt that may be broadly classified as inhibition of anion absorption, surface roughening, electronic factors [29]:

(i) Structure sensitive inhibiting formation of OH_{ads}. It is well known that in high-surface-area Pt/C dispersed catalysts, the dominant Pt crystal faces that are exposed are <111> and <100>. The <1 1 1>, <1 0 0> & <1 1 0> surfaces are increasingly active in that order for sulfuric acid and <1 0 0>, <1 1 0> & <1 1 1> for perchloric acid. Some studies have shown that Pt_3Co alloys have activities that are several times that of polycrystalline Pt which was attributed to the inhibition of OH_{ad} formation on the Pt in the alloys.

(ii) Surface roughening. Studies have suggested that surface roughening of the Pt alloy takes place due to dissolution or leaching of the more oxidizable base-metal in bulk alloys leading to higher activity via an increase in surface area.

(iii) It has been demonstrated that alloying of Pt with transition metal increased the Pt d-band vacancy.

For the purpose of this thesis we have alloyed platinum with cobalt and analyzed some of the above mentioned hypotheses by comparing the changes in the electrochemical and ORR activities of the catalyst before and after alloying.

2.3.4 Kinetics of O_2 Reduction Reaction

In a PEMFC, it is desirable to have the O_2 reduction reaction at potentials as close as possible to the thermodynamic electrode potential (i.e., with less overpotential) with a satisfactory reaction rate. If the overpotential is large, the backward reaction is negligible and the ORR kinetics can be described as

$$I_c = i^0_{O_2} e^{\frac{n_{\alpha O}\alpha_O F \eta_c}{RT}} \tag{2.8}$$

The plot of η_c ~ log (I_c) gives a linear relationship, and the slope is $\frac{2.303RT}{\alpha_o\, n_{\alpha 0} F}$. This slope is called the Tafel slope. Since all the parameters in the Tafel slope are known, the parameters determining the Tafel slope are actually α_o and $\eta_{\alpha o}$. Figure 2.6 shows an example of a Tafel plot. The higher the Tafel slope, the faster the overpotential increases with the current density. Thus for an electrochemical reaction to obtain a high current at low overpotential, the reaction should exhibit a low Tafel slope or a large $\alpha_o\eta_{\alpha o}$. The electron transfer coefficient is a key factor determining the Tafel slope [26].

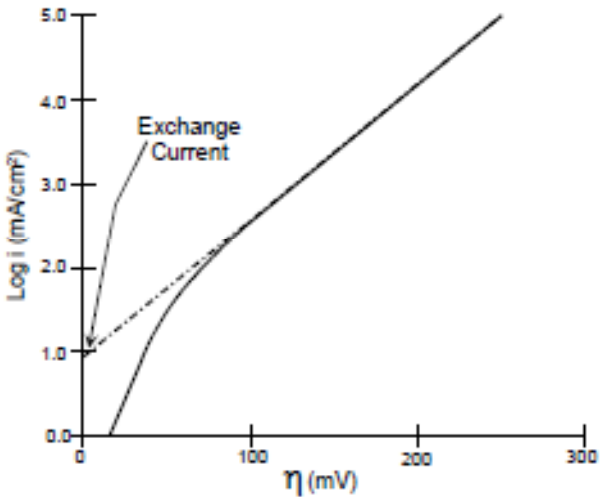

Figure 2.6 Example of a Tafel Slope

2.3.4.1 Exchange Current Density

Exchange current density is an important kinetic parameter representing the electrochemical reaction rate at equilibrium. For an electrochemical reaction,

$$O + ne^- \leftrightarrow R \tag{2.9}$$

both forward and backward reactions can occur. At equilibrium, the net current density of the reaction is zero. The current density of the forward reaction equals that of the backward reaction. This current density is called exchange current density. The magnitude if the exchange current density determines how rapidly the electrochemical reaction can occur [26]. Figure 2.6 shows the determination of exchange current density from Tafel plot.

CHAPTER 3

EXPERIMENTS

3.1 Synthesis of Catalysts

3.1.1 Preparation of Pt/C Catalyst

$Pt(acac)_2$ was first dissolved in Acetone (electronic use grade, residue free) at room temperature to obtain a transparent solution. Ketjen carbon black (EC300J, Akzo Nobel Chemicals), in an amount corresponding to 20wt% of Pt on carbon, was then slowly added. The mixture was treated by ultrasonication (Fischer Scientific FS30H) for about 15 minutes to achieve better homogenization and allow $Pt(acac)_2$ to adsorb on the carbon supports. Adsorption was further enhanced by shaking the solution in a mechanical mixer (Spex SamplePrep 8001) for 1.5 hr. The mixture was subsequently allowed to dry at room temperature under mild mechanical agitation and with controlled evaporation rate. Once the solvent was completely removed from the mixture, the Ketjen carbon black with the adsorbed $Pt(acac)_2$ was grounded using an Agate motar and pestle in inert atmosphere. Highly dispersed Pt/C catalysts were obtained through thermal decomposition of the adsorbed $Pt(acac)_2$ in a quartz tube furnace (Thermolyne 79300) according to the temperature profile shown in Figure 3.1. The synthesized sample was also subjected to annealing (heat treatment) in order to improve the surface morphology of the Pt particles. During the heat treatment, temperature was increased at a rate of 20ºC/min with Argon flow and then held for 2 hr at about 600˚C to remove any volatile impurities that may be present on the surface of the catalysts, and also to improve the surface properties of the Pt/C catalyst. After the annealing, the Pt/C catalysts were allowed to cool naturally.

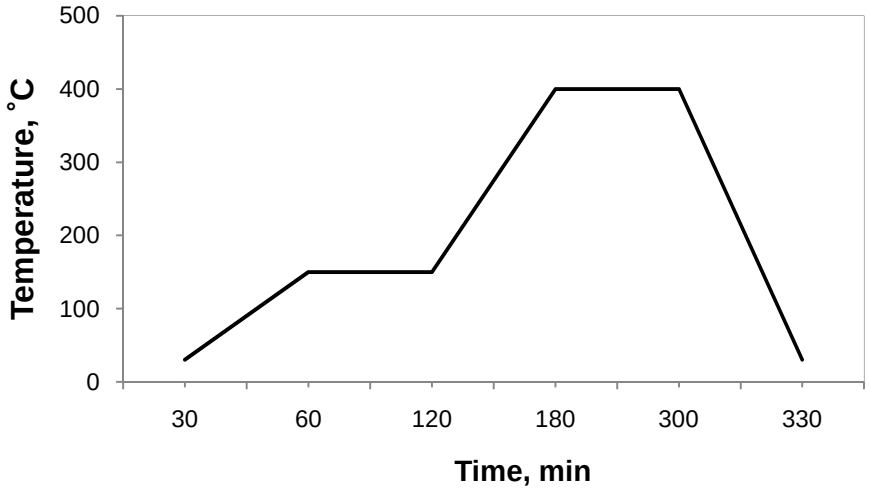

Figure 3.1 Temperature profile for heat treatment during one-step synthesis Pt nanoparticles.

3.1.2 Preparation of Pt_3Co/C Catalyst

The process for synthesizing 20%Pt_3Co/C was similar to that of the Pt/C catalyst. Pt $(acac)_2$ and Co $(acac)_2$ were taken such that the Pt to Co remains an atomic ratio of 3:1. The heating profile for 20% Pt_3Co/C is as shown in Figure 3.2. The heat treatment (annealing) was performed in a tube furnace in the presence of Argon to prevent the Carbon Black from oxidizing, similar to Pt/C catalyst with a heating rate of 10ºC/min, the temperature was at 800C for about 2 hours, and then the catalyst was allowed to cool naturally at room temperature. Here a higher temperature was used to ensure alloying between Pt and Co.

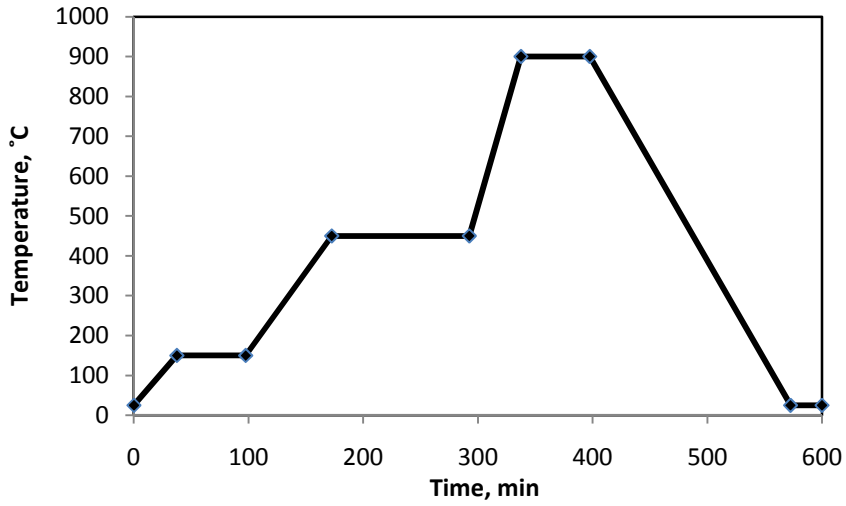

Figure 3.2 Time vs. Temperature for Pt_3Co/C catalyst synthesis

3.2 Electrochemical Testing

3.1.2 Disk Electrode Technique

Rotating disk electrode (RDE) method has been widely used for electrochemical analysis and evaluation as it can ensure an electrode reaction under well- hydrodynamic conditions [26]. With the recent development of PEM fuel cells, it has been widely employed to screen the activity of some electrocatalysts (e.g. Pt-based, non-noble catalysts) towards fuel cell reactions, such as oxygen reduction, hydrogen oxidation, methanol oxidation and CO tolerance in simulated fuel cell environments.

The two types of RDE configuration commonly used in study of PEM fuel cells are, thin film RDE and porous RDE. Porous RDE (Figure 3.3) can be usually prepared by spreading a certain amount of catalyst ink onto a glassy carbon disk, after which the catalyst-ink-covered disk is dried at room temperature to evaporate the solvents. The thickness of the catalyst layer formed is calculated approximately according to the loading and density of the catalyst, and the area of the glassy carbon electrode. The catalyst ink is usually prepared by mixing the electrocatalyst, electrolyte (e.g. Nafion) and the solvent in a certain ratio. In this method, the glassy carbon disk can be covered by a single layer, in which the catalyst and the electrolyte are homogenously distributed. In the case of a thin-film RDE, the glassy carbon disk is usually

covered by two layers. The first layer is the catalyst (inner layer) and the second of Nafion (outer layer). In this method the reactants (O_2 or H_2) first diffuses through the Nafion film and then reacts at the catalyst surface. This thesis adopted the former RDE type.

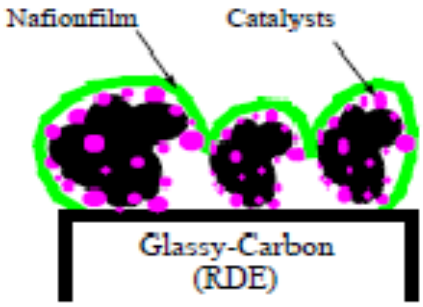

Figure 3.3 A schematic view of the electrode surface used in a cyclic voltammeter [31].

3.2.2 RDE Preparation

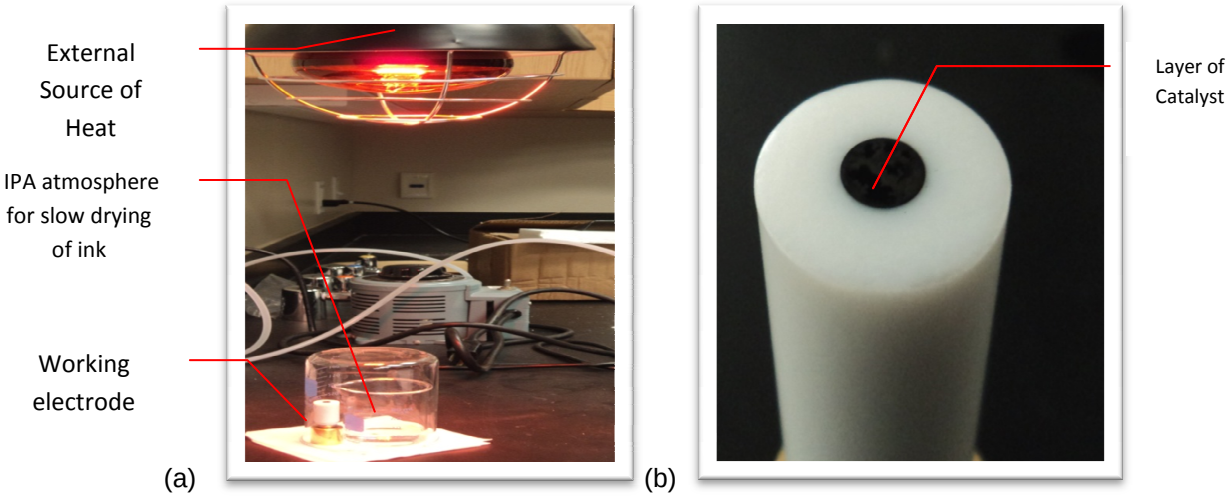

Figure 3.4 (a) Electrode coating by subjecting the catalyst ink on the electrode surface to an Infrared lamp & (b) is the catalyst coated working electrode.

Catalyst inks were prepared by mixing 0.015g catalyst (46.7wt% TKK *TEC10E50E* or the in-house synthesized 20%Pt/C & 20% Pt_3Co/C catalysts) with 12 ml DI water (from Millipore Simplicity water purifier), 3 ml of isopropanol (IPA), and 60 µl of Nafion solution (Ion Power Inc.). According to references [32, 33], the mixture was first homogenized for 15 to 20 minutes in an utlrasonicater (Fischer Scientific

FS30H) and 15 µL of the mixture was then deposited onto the electrode surface. For the initial 5-8 minutes the electrode was placed under an infrared lamp until the drop appeared flat, after which the electrode was allowed to dry under ambient conditions. This method prevented over drying of the coated layer and therefore rendered uniform coating with less cracks, therefore ensuring better repeatable results.

3.2.3 Cyclic Voltammetry

All the cyclic voltammetry (CV) tests were carried out using Applied Princeton Research PARSTAT 2273 advanced electrochemical system in a three electrode configuration (Figure 3.4), consisting of a rotating disk electrode (RDE) with a glassy carbon as the working electrode, a Pt mesh as the counter electrode, and a Standard Hydrogen Electrode (SHE) as the reference electrode. CV data was obtained in 0.1M $HClO_4$ electrolyte before purging with Argon for at least 20 minutes to completely remove oxygen. The potential scan was carried out at a rate of $20mVs^{-1}$ in the range of 0.03V to 1.2V. After the scan was stabilized during the first 10-30 cycles, CV curves were recorded. All the CV curves are plotted against the SHE. Calculation for was performed by using the hydrogen adsorption peak (area under the reduction part of the curve) [34].

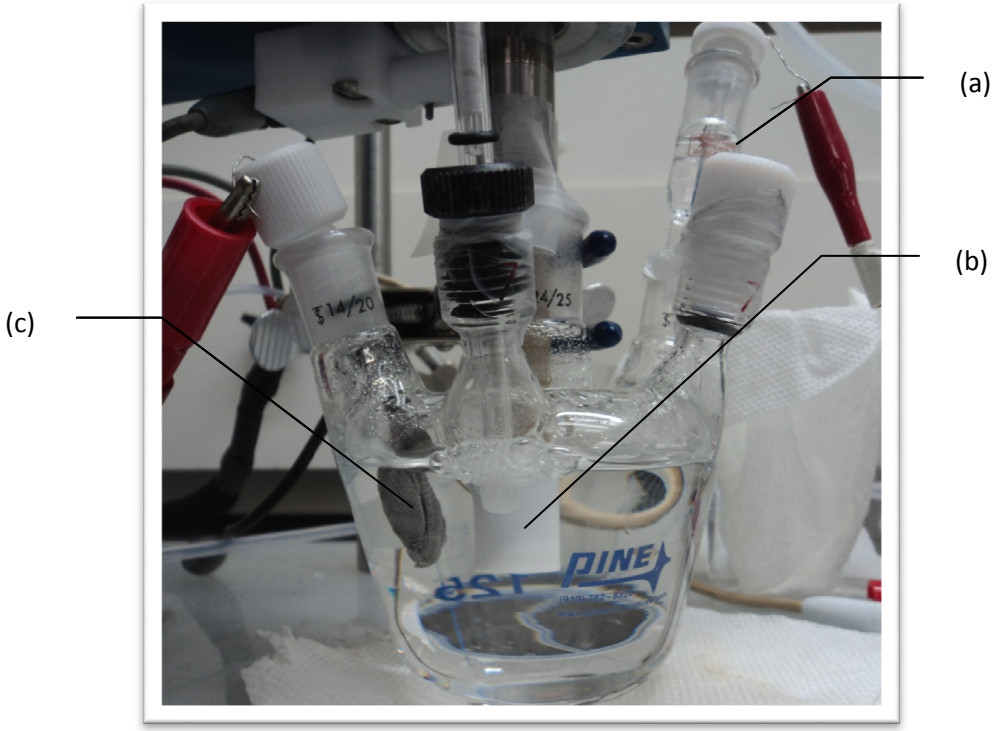

Figure 3.5 Three electrode set up for cyclic voltammetry, consisting of a) Working electrode, b) Counter electrode & c) Reference electrode.

To evaluate ORR kinetics, the electrolyte solution was saturated with pure oxygen for about 20 minutes before the hydrodynamic voltammograms were obtained. The ORR results were recorded in the potential range of 0.2 V to 1.08V in order to prevent oxidation of carbon at 1.2V [35] and at rotation speeds in the range of 400 rpm to 2500 rpm. The durability tests were performed in 0.1M $HClO_4$ electrolyte solution. The catalysts were subjected to recurrent potential cycles – 0.6 V (5s) and 0.95 V (5s) – for about 20,000 cycles (i.e., 56h). At the end of every 5000 cycles the electrolyte solution was replaced and the CV and ORR curves were collected in order to obtain the electrochemical degradation.

3.2.4 Electrochemical Reactions in Cyclic Voltammetry

Catalyst surface area and poisoning effects can be evaluated from the CV curves. Before taking the CV tests, it is important to ensure the electrode is wet thoroughly to access the catalyst completely. The electrode is then mounted in the holder placed in the cell and swept from about -0.02V to 1.2V in either

0.1M perchloric acid or 0.5M H_2SO_4. An example of CV obtained for surface area determination is shown in Figure 3.5.

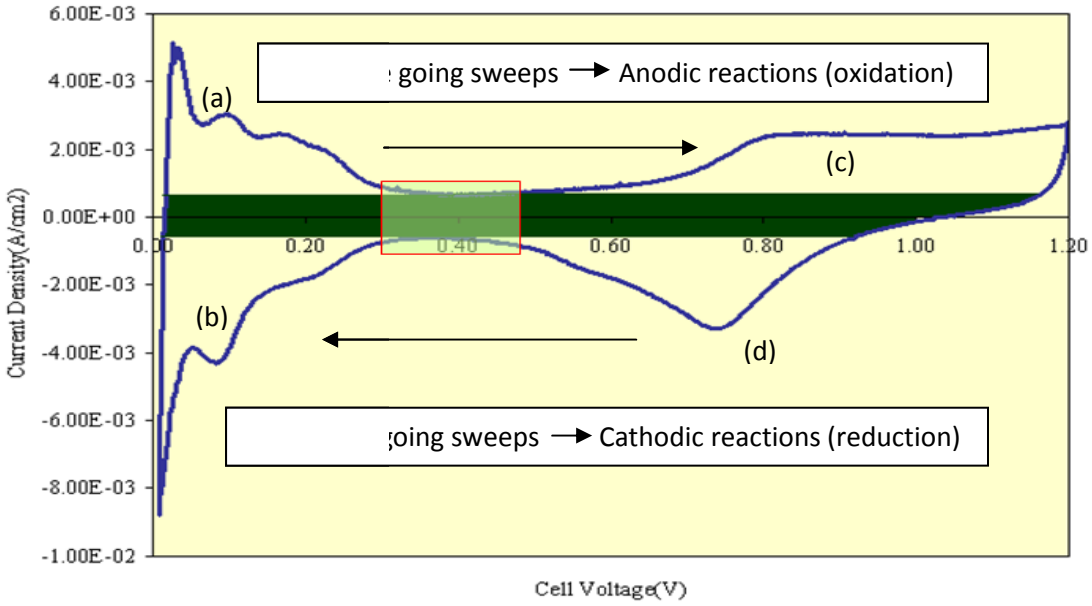

Figure 3.6 Typical Pt based cyclic voltammogram representing the anodic and cathodic sweeps; (a) Region of H_2 desorption and oxidation, (b) H_2 adsorption and evolution (c) Pt oxide formation & (d) Pt oxide reduction.

Figure 3.6 a), b), c) & d) signify the hydrogen adsorption/desorption and Pt oxidation/reduction reactions, respectively, occurring on the Pt nanoparticles surface embedded in the carbon substrate on the working electrode surface. In order to evaluate the electrochemical surface area (ECA), we integrate the area under the peak marked as (b) in Figure 3.5, i.e., from the double layer to the second minimum in reduction current before the onset of hydrogen evolution. Alternatively, the hydrogen desorption area (Figure 3.6 (a)) up to -0.03V (vs. RHE) can also be used for integration. The hydrogen adsorption charge calculated from the area under the curve is converted to surface area using the value of 210 µC (one H per Pt atom) per square centimeter of platinum surface [36].

3.2.4.1 Determination of ECA from the Charge Density of Pt

Pt catalyst nanoparticles have an fcc cubo-octahedral 3D geometry (Figure 3.7) with eight (111) and six (100) faces. Moreover, catalytic properties vary significantly from the atoms located on the faces to those located on the edge or corners of the nanoparticles [37].

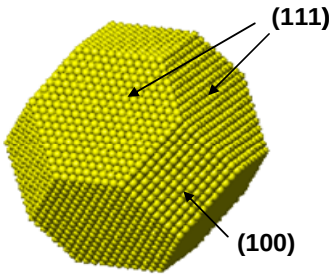

Figure 3.7 FCC (face-centered cubic) cubo octahedral crystalline structure of Pt nanoparticles.

The Pt (100) is the most active face in perchloric acid toward ORR. Therefore we determine the planar density of platinum based on (100) crystal plane as follows:

(a)

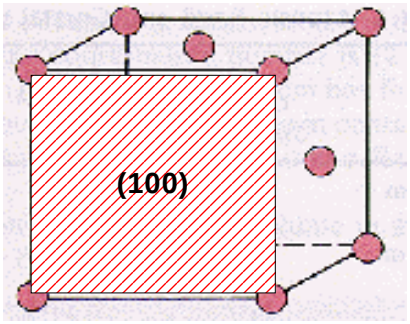

(b)

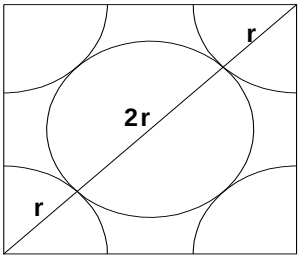

Figure 3.8 a) & b) Schematic of Pt fcc structure

$$a^2 + a^2 = (4r^2) \quad (3.1)$$

$$a = 2\sqrt{2}r \quad (3.2)$$

$$r = 1.39\ \text{Å} \quad (3.3)$$

$$a = 3.92\text{Å}$$

Number of atoms per unit area = 1 atoms + 4 atoms x ¼ **= 2**

$$\rho = \frac{2\ atoms}{(3.92\ \text{Å})} = 1.3 \times 10^{15}\ \textbf{atoms/cm} \tag{3.4}$$

3.2.5 Catalyst Activity

In an electrochemical reaction, the exchange current density and Tafel slope together define the activity of the catalyst. Due to difficulties and uncertainties of these parameters for a RDEl electrodes, alternative ways of defining catalyst activity of fuel cells have be adopted in this thesis. These include: mass activity, specific activity, and catalyst utilization.

(a) Mass Activity is defined as follows:

$$A_w = \frac{i_{0.9}}{W} \tag{3.5}$$

where A_w is the mass activity of the catalyst, $i_{0.9}$ is the current density in **mA/cm^2** at 0.9V, and **W** is the loading of platinum in **mg/cm^2**. The value of 0.9V is chosen to avoid inclusion of any concentration polarization. The mass activity is measured under saturated oxygen in the electrolyte as the reactants. In order to calculate the mass activity, polarization curve for a given electrode is established. The current density at 0.9 V is obtained from current-potential data [36].

(b) Specific Activity is defined by:

$$A_s = \frac{i_{0.9}}{Sr} \tag{3.6}$$

Where, A_s is the specific activity of the catalyst and S_r is the real (accessible) ECA of the catalyst in the electrode in **cm^2**. The accessible surface area of the catalyst is determined using the methods described.

CHAPTER 4

RESULTS AND DISCUSSION

4.1 Pt/C Catalysts

4.1.1 Adsorption Isotherms

Pt loading of the Pt/C catalysts depends on the amount of precursors adsorbed on the carbon support. Following the similar adsorption isotherm calculation in [38] and assuming the projected diameter of each $Pt(acac)_2$ molecule is 0.27nm (center-to-center distance of the atoms in the molecule), Ketjen black with surface area at around $850m^2/g$ is found to theoretically provide 57wt% Pt/C at maximum adsorption capability. However, unlike the sc-CO_2 deposition where the adsorption critically depends on the equilibrium between precursor uptake and solution concentration, maximum adsorption is guaranteed in this work since the solvent is eventually totally evaporated. The complete adsorption also relies on the strong adsorbate-adsorbent interaction (whether short-range or long-range), as observed in many studies [39, 40]. Experimentally measured loading of the synthesized Pt/C, conducted by thermal gravimetric analysis (TGA) in air, as successfully demonstrated in reference [41], confirmed that the yield of Pt nanoparticles can be as high as ~95%.

4.1.2 XRD analysis on Pt catalysts

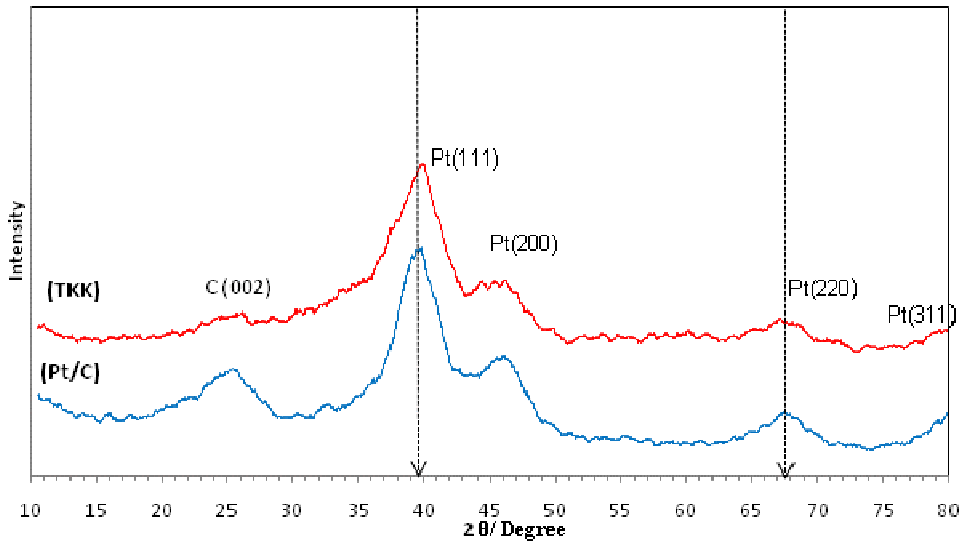

Figure 4.1 XRD results for the synthesized Pt/C & TKK catalysts

Figure 4.1 shows the XRD patterns of the synthesized 20wt% Pt/C and 46.7wt% TKK catalysts. The diffraction peak at 2θ=25º is a characteristic peak (002) for Ketjen carbon black [42]. The figure also indicates that the Pt on the Ketjen black substrate is a face centered cubic (fcc) structure and has major peaks at 2θ=39.5º (111), 2θ=45.5º (200), 2θ=67.4º (220) and 2θ=81.4º (311). The mean particle size for the synthesized Pt/C calculated from the (220) peak using the Scherrer Equation [43] is found to be similar to that of the TKK catalyst at ~2.6nm.

Table. 4.1 Mean Particle Size of the synthesized Pt and TKK catalysts

Catalyst	Particle size, nm
20% Pt/C	2.66
TKK	1.69

4.1.3 HR-TEM to study the Particle size and size distribution

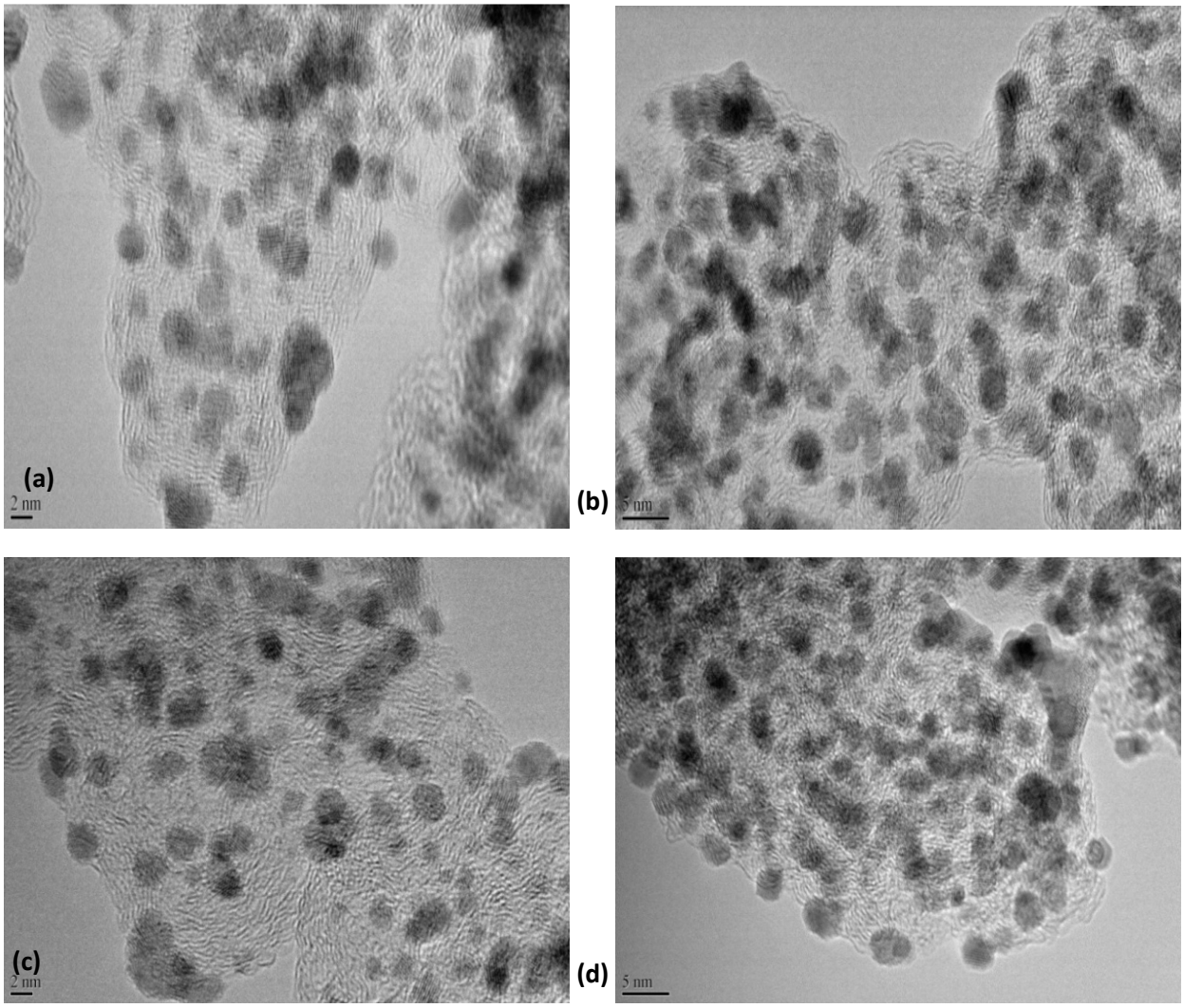

Figure 4.2 HR-TEM Images for a), b) the synthesized Pt/C; and c), d) commercial TKK catalysts.

Figures 4.2 a, b, c and d show the HR-TEM images (Hitachi H-9500) of the synthesized and TKK Pt/C catalysts at different magnifications. The carbon support and Pt particles are easily identified from the TEM images. Pt particle agglomeration can also be observed for both samples. It can be seen that the two samples have similar particle size and shape, i.e., spherical particles with size ranging from 1 to ~4nm. Due to limited resolution of the TEM machine, detailed examination on particle surface morphologies has not been attempted.

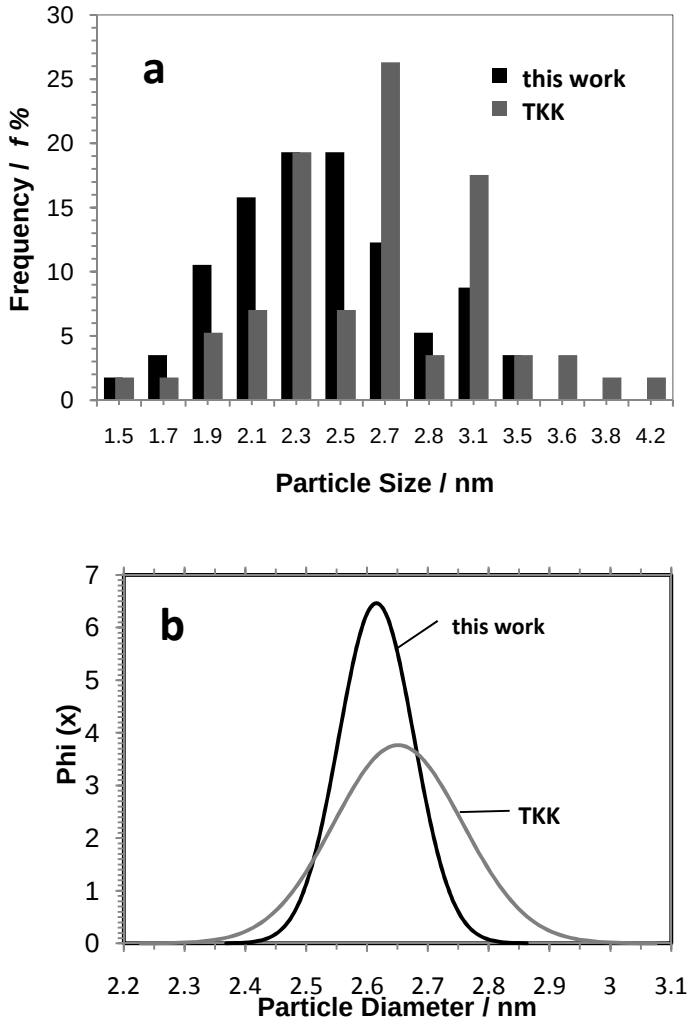

Figure 4.3 Particle size distribution for the synthesized Pt/C in this work and TKK Pt/C: a) calculated based on ~70 particles selected from HR-TEM images, and b) assumed normal distribution calculated from standard deviation and mean.

From the HR-TEM images, around 70 representative Pt particles were chosen, and the mean particle size and standard derivation of the two samples were calculated. The calculated particle size distribution is shown in Figure 4.3 a) and a standard (normal) distribution curve is displayed in Figure 4.3 b. Clearly, both curves show that the synthesized catalyst has slightly smaller particle size and narrower distribution. The average particle sizes as calculated from the HR-TEM are 2.6 nm and 2.65 nm for the in-house synthesized Pt/C and TKK catalysts, respectively. The standard deviation of the particle size is 0.061 for the synthesized Pt/C catalyst, about half of that of the TKK catalyst.

4.1.4 EDX Images to detect the presence of Pt

In order to qualitatively measure the amount of Pt in the synthesized catalyst and corroborate the theoretical amount of Pt content in the catalyst, EDX measurements were taken as shown in Figure 4.4 and the amount of the Pt recorded in the catalyst samples was calculated to be ~20%. The calculated amount of Pt in the sample correlates well to the amount of Pt quantified via EDX, due to high yield of the one-step synthesis.

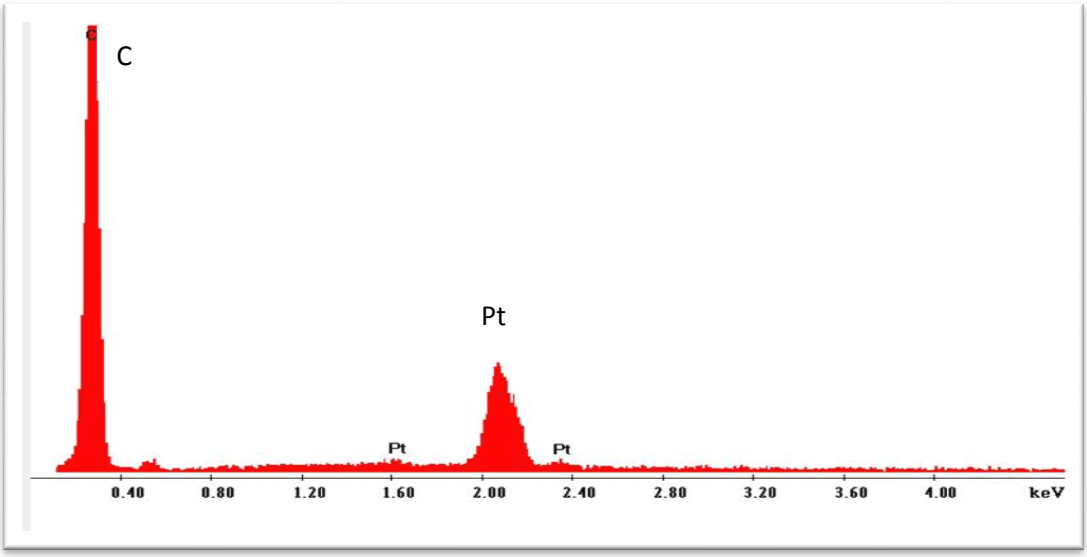

Figure 4.4 EDX Image of Pt catalyst nanoparticles

4.1.5 Electrochemical Characterization

4.1.5.1 Cyclic Voltammograms

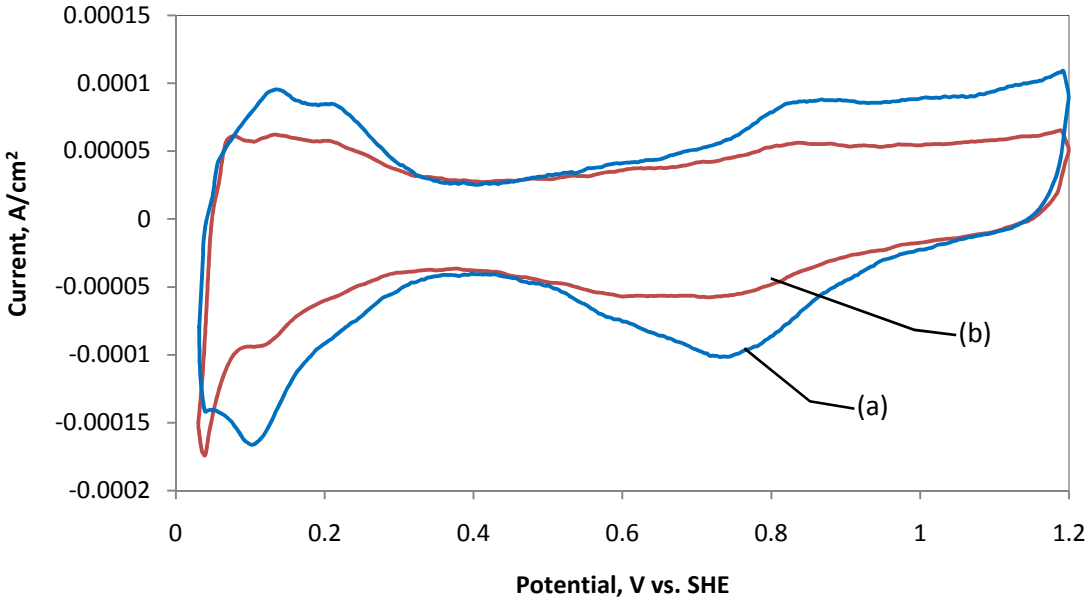

Figure 4.5 CV curve for a) TKK & b) Pt/C catalyst

Figure 4.5 is a comparison between the CV curves obtained for the synthesized sample Pt/C & commercial sample TKK. The purpose of the cyclic voltammetry experiments was to (a) determine the ECA of the electrode coated with the respective catalyst, (b) detect the presence of any form of contamination and (c) analyze any changes in the structural or intrinsic properties of the catalyst.

The ECA is defined as the “real" catalyst surface area per mass of catalyst (e.g., m^2/g_{Pt}) in contact with both the electrolyte phase as well as the electronic phase. ECA is determined using cyclic voltammetry where the electrolyte was purged with Ar so that only the surface reactions involving electrolyte were measured. The voltage of the cell was changed at a constant rate (i.e., dV/dt= r where *r* is the scan rate and t is the time) of 20mV/s. The cell current density was measured and plotted vs. the cell voltage. The plot is referred to as *cyclic voltammogram*.

It is important to ensure a good contact between catalyst support (carbon) and catalyst particles obtain a high ECA value. Some of the other key factors such as carbon support surface area, Pt particle size, Pt weight fraction and Pt composition, can be optimized in order to achieve high ECA value.

The ECA in m^2/g_{Pt} is calculated from the hydrogen adsorption and desorption peaks in the CV curves using the following relation [19],

$$\mathrm{ECA} = \frac{Q_H}{[\mathrm{Pt}]Q_c} \qquad \textbf{[4.1]}$$

where Q_H (mC/cm^2) is the charge transferred under the hydrogen peaks involving one electron/platinum stoichiometry, [Pt] the Pt loading in the working electrode, and Q_C the electrical charge associated with a monolayer adsorption of hydrogen on Pt (0.21 $\mu C/cm^2$) [25]. For the given samples, the ECA of the catalysts were determined and tabulated as follows

Table 4.2. ECA values for the synthesized and commercial catalyst

Samples	ECA (m^2/g)	
	Adsorption	Desorption
Pt/C	87.3	62.1
TKK	60.85	42.41

From the particle size analysis data it was found that the particle size of Pt/C and TKK were almost identical (~ 2.6nm). The higher ECA value observed for the synthesized catalyst may be attributed to narrower size distribution of the Pt nanoparticles compared to that of the TKK. Large particles in the 'tail' toward higher size for the commercial catalysts (Figure 4.2) reduce availability of Pt for adsorption and desorption of hydrogen.

In order to estimate the amount of Pt surface area that was utilized for electrochemical activity by Pt particles that fell in the range of ~2.6nm, the theoretical surface area of Pt particles was calculated. It was found that the contribution of Pt particles in the range of 2.6nm which assume the stable cubo-octahedral

structure at equilibrium towards the electrochemical activity for TKK was ~103.9 m^2/g_{Pt} and ~104.7 m^2/g_{Pt} for the synthesized Pt/C catalyst.

4.1.5.2 Accelerated Durability Tests

In this study, a commercial TKK catalyst with higher Pt loading (46.7wt%) than the synthesized Pt/C (20wt%) was used as a baseline. It is well-known that Pt loading on the carbon support greatly influences particle size and agglomeration. However, it was recently reported that the properties of the carbon support seem to have dominating effects on performance and stability of the Pt catalysts [44], depending on whether the carbon surface structures are graphitized or amorphous. Though the TKK catalyst has different Pt loading, it is still considered as an appropriate baseline as it has the same carbon supports – Ketjen black – as the synthesized Pt/C. Other commercially available 20wt% Pt/C catalysts, e.g., from E-TEK (now Basf Corp.), do not use Ketjen black as the support.

One of the major degradation modes of hydrogen fuel cells under automotive conditions is Pt dissolution and ECA loss. It is expected that the two catalysts with different particle size and distribution would have different electrochemical characteristics such as ECA, ORR activity, and electrochemical durability. The ORR activity and electrochemical degradation of the synthesized Pt/C were studied in comparison to those of the TKK catalyst. Figures 4.6 a and b show the variation of the CV curves for the two samples during the recurrent potential cycles in the range of 0.6 V (5s) to 0.95 V (5s) up to 56 hr (or 20,000 cycles). Characteristic carbon peaks, caused by the quinone-hydroquinone reaction in 0.4 – 0.8V, become more significant after 5k cycles for both samples. The integrated areas under those carbon peaks after 20k cycles are estimated to be several times larger than the initial ones, mainly due to the accelerated carbon corrosion by Pt [45].

A significant increase in the electrical double layer is also observed from the CV curves of both samples. The increased double layer could be due to the emergence of multiple functional groups such as —C=O (ketones) at lower potentials or —O-C (ether) groups present at higher potentials. Kinoshita [46] provided detailed explanations of these changes in carbon structures at certain potentials during similar potential cycles. The results in Figure 4.6 clearly indicate the importance of carbon supports in evaluating catalyst durability, as the Pt-catalyzed carbon corrosion is critically dependent on

physicochemical properties of carbons. Since the two samples have the same carbon support, i.e., Ketjen black, a relative comparison in catalyst degradation is easy to make.

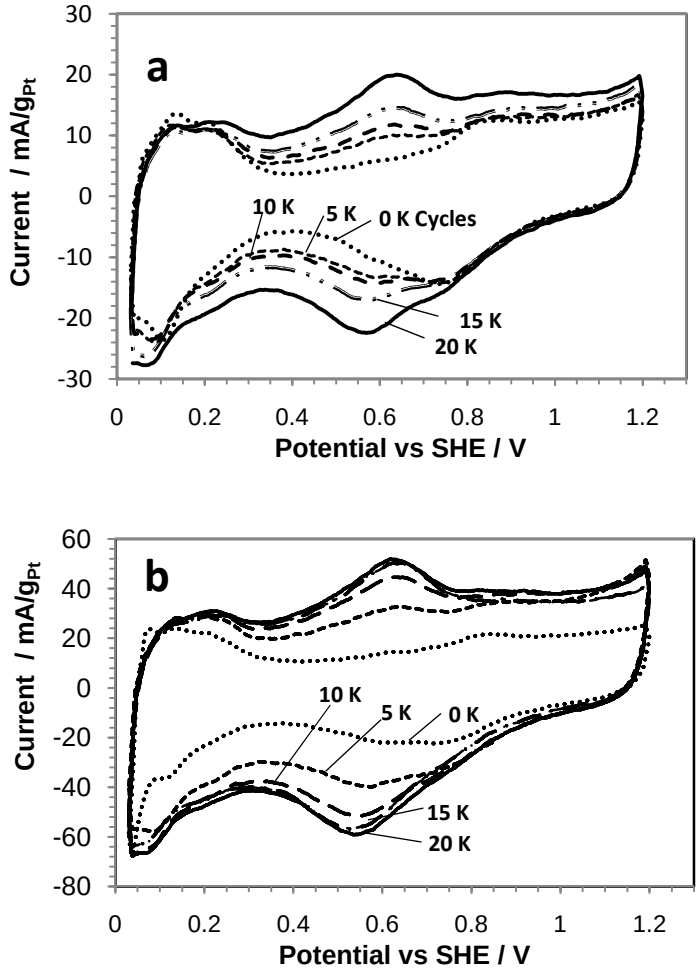

Figure 4.6 CV curves during potential cycles for a) commercial TKK catalysts, and b) the synthesized Pt/C. The catalysts were subjected to recurrent square-wave potential cycles, i.e., 0.6 V (5s) and 0.95 V (5s).

4.1.5.3 Infrared Spectral Data

The increasing anodic peak observed at ~0.6V and the cathodic peak at about ~0.55V with potential cycles (Figure 4.6), are associated with the oxidation and reduction of functional groups on the surface of carbon [46]. In order to verify the presence of these oxide or functional groups, FT-iR spectra for the blank carbon sample as well as the synthesized Pt/C were obtained in Figure 4.7.

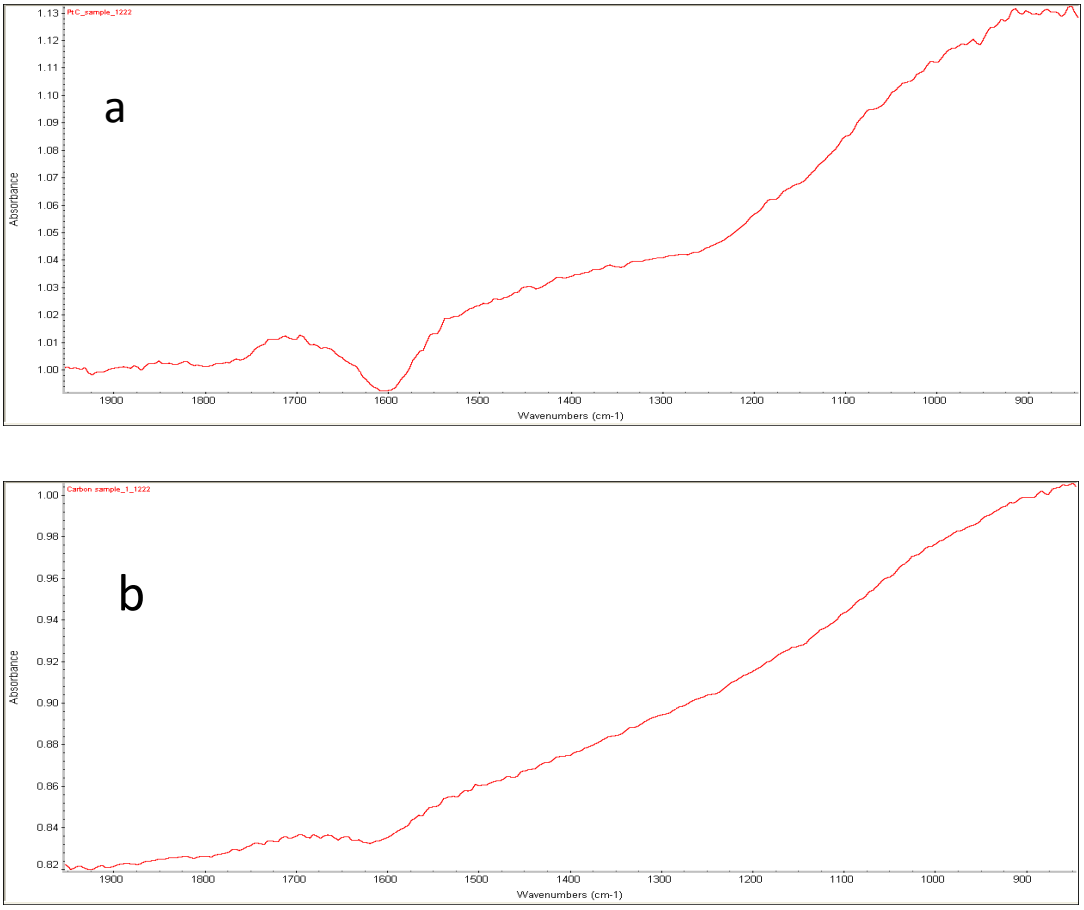

Figure 4.7 Ft-iR spectra of a) Pt/C & b) Ketjen carbon black

The adsorption bands obtained at 1600cm^{-1}, identified for both samples, is attributed to carbonyl stretching frequencies for carboxylic and quinone groups (organic compounds containing 2 carbonyl groups), respectively [46]. During the accelerated durability tests, it was observed that the electrochemical oxidation on the carbon surface showed an increase in the anodic and cathodic currents

associated with the redox couple (quinone/hydroquinone) with potential cycling. Numerous researchers, have ascribed these redox processes on carbon to the electrochemical reactions of surface oxide groups [46].

4.1.5.4 ECA Decay Rate

Figure 4.8 shows the normalized ECA decay rate during potential cycles for the two samples. The initial ECA value recorded for the synthesized Pt/C catalyst is $87.3 m^2/g_{Pt,}$ which is higher than that of the TKK catalyst at $60.85 m^2/g_{Pt}$. We notice that the measured ECA for the TKK catalysts is smaller than the reported values (for example, see the benchmarked activities by GM [29]). This is probably because we ran the same number of potential cycles for both the TKK catalysts and the in-house synthesized Pt/C before the initial CV curves were taken, to ensure fair comparison, though it took longer for the synthesized Pt/C catalyst to become stabilized. It was found that the synthesized catalysts were more hydrophobic as demonstrated by a larger contact angle when water droplets were placed onto the RDE. The 'initial' ECA for the TKK catalysts is thus the value after a period of potential cycles (10-30 cycles). Other factors contributing to the higher ECA of the synthesize Pt/C can be attributed to smaller particle size and narrow size distribution, as evidenced in Figure 4.3. Detailed investigation on the surface wettability of the synthesized Pt/C is currently underway.

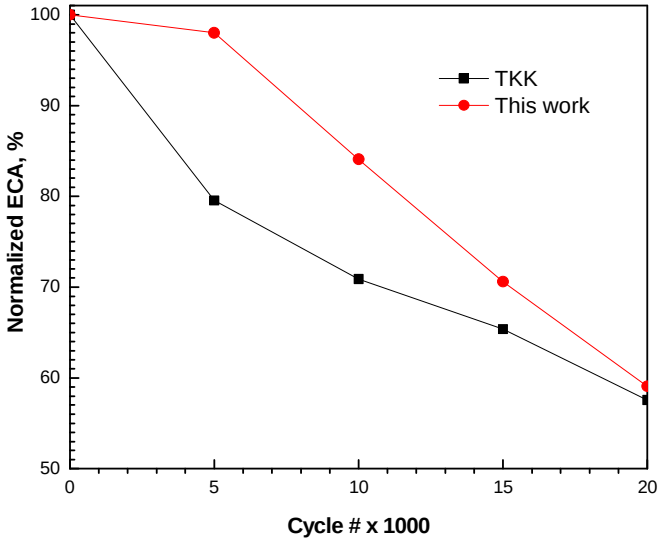

Figure 4.8 Comparison of ECA loss for the synthesized and TKK Pt/C catalysts during potential cycles. The initial ECA values are 60.85 and 87.30 m^2/g_{Pt} for the TKK and synthesized Pt/C catalysts, respectively.

Figure 4.8 shows that the ECA of the synthesized Pt/C remains almost unchanged after the initial 5k cycles, followed by a steep linear decrease from 5k to 20k cycles. During the initial cycles, it is hypothesized that an increased contact between the Pt and electrolyte, due to an improved wetting of the synthesized Pt/C catalyst (because of its hydophobicity), is able to cancel the ECA loss due to potential cycles. But once the Pt/C particles became completely wetted by the electrolyte solution, the surface area started to decrease significantly. This is because during the potential cycles, the catalysts were exposed to a corrosive environment, and Pt atoms, especially at the edges and corners, began to corrode resulting in a loss of the active surface area [47]. Different mechanisms of Pt dissolution-redeposition on the catalyst surface and Pt migration through the surface have been suggested [47] in the literature to explain the increase of the catalyst particle and decrease of ECA with time. At 20k cycles the synthesized catalyst still shows higher decay rate (examined from the slopes as indicated in Figure 4.8), probably owing to smaller particle size. But the in-house synthesized Pt/C is able to maintain its higher ECA value even after the 20k potential cycles. The TKK catalyst has similar ECA loss within the entire 20k cycles, but during the first 5k cycles the ECA decreases by about 20% before slowing down at about 10k cycles.

4.1.5.5 ORR Polarization

Figure 4.9 shows the ORR current obtained in 0.1M $HClO_4$ at room temperature and 1600 rpm for the TKK and synthesized catalysts at the same catalyst loading (but with different Pt loadings). The area-based limiting current, solely dependent on the solution-phase O_2 diffusion rate, is similar for the two catalysts. In Figure 4.9 the current has been normalized to the Pt mass on the RDEs, for the purpose of showing the activity on Pt mass basis. From the plot it is observed that the limiting current in A/mgPt for the synthesized sample almost doubles that of the TKK catalysts, although the geometric-area specific currents are similar for the two samples. Since the two catalysts have different Pt loadings, it is more meaningful to compare the relative decay rate rather than the absolute activity values.

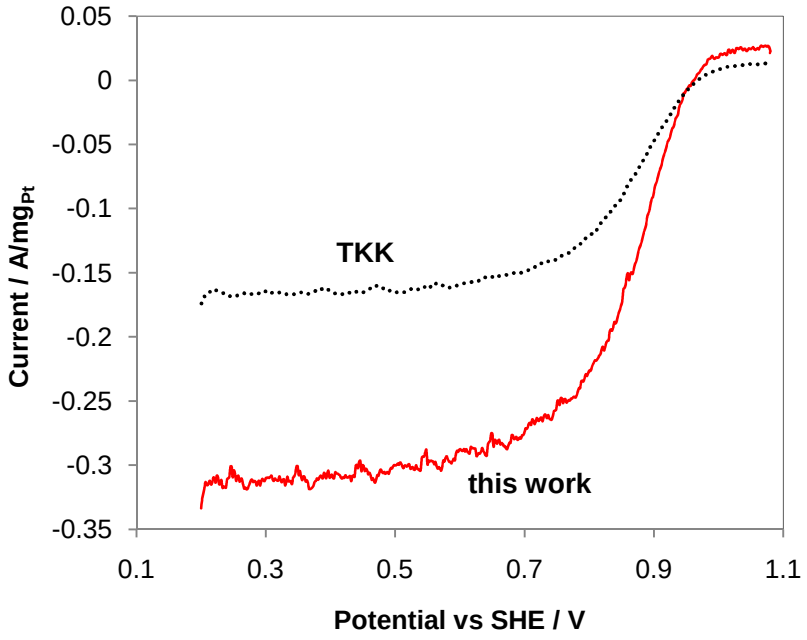

Figure 4.9 A comparison of the initial ORR polarization curves during the anodic sweep in RDE measurements between the synthesized and TKK Pt/C catalysts in 0.1M $HClO_4$ at 1600rpm and sweep rate of 20mV/s.

4.1.5.6 Catalytic Activity

In order to estimate the mass and specific activity of the catalysts, kinetic currents are calculated from the well known mass-transport correction for rotating disk electrodes [48], i.e.,

$$i_k = \frac{i_d i}{i_d - i} \qquad \textbf{(4.3)}$$

where ***i*** is the experimentally obtained current at 0.9V, $\boldsymbol{i_d}$ refers to the measured diffusion-limited current, and $\boldsymbol{i_k}$ is the mass transport kinetic current [29]. The normalized mass activity is plotted against the cycle number in Figure 4.10.

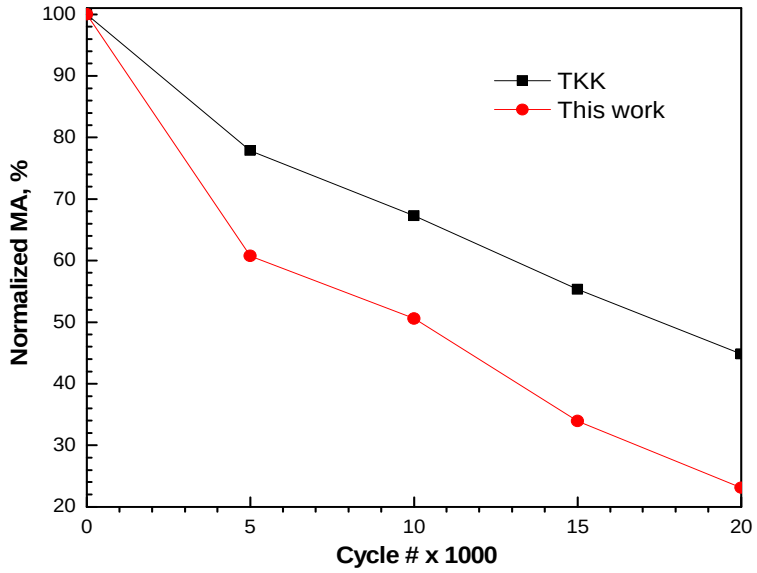

Figure 4.10 Decay of mass activity with time during potential cycles for the synthesized and TKK Pt/C catalysts. The measurement was taken in O_2-saturated 0.1M $HClO_4$ with a scan rate of 20mV/s. The initial mass activities are 0.067 and 0.12 A/mg_{Pt} for the TKK and synthesized Pt/C catalysts, respectively.

The initial mass activity and specific activity values obtained are tabulated in Table 4.3. The initial mass activity of the synthesized sample seems higher by a factor 2 than that of the TKK Pt/C (0.12 vs.

0.067 A/mg_{Pt}); however, the synthesized catalysts experience a much quicker decay, especially during the first 5k cycles. After 5k, the two curves become parallel indicating similar degradation rate.

Table 4.3 Initial ORR activity of synthesized and commercial samples

Samples	$i_{m,}$ mA/µg	$i_{s,}$A/µcm^2
Pt/C	0.12	137.85
TKK	0.067	109.89

Figure 4.11 shows the specific activity loss of the two samples during potential cycles. The specific activity is primarily dependent on the ECA and mass activity with the relationship – SA=MA/ECA. The specific activity is fairly stable for the TKK catalysts within the 20k cycles. The in-house synthesized Pt/C initially displayed a significant drop (close to 40%) in specific activity, owing to a flat ECA decay and large mass activity loss as shown in Figures 4.8 and 4.10, respectively. The specific activity loss seems stabilized and becomes parallel to that of the TKK catalysts after 5k cycles.

The observed differences in activity and ECA losses between the synthesized Pt/C and TKK catalysts may be attributed to different surface morphologies. For the assumed cubo-octahedron structure [49] of Pt nanoparticles (though any accurate representation of Pt nanoparticles using a well-defined geometric model is in debate), Kinoshita suggested that [50] the mass and specific activity can be correlated to the fraction of surface atoms on low-index crystal faces, such as (111) and (100). It was also demonstrated that a maximum mass activity was found for the particles with size ~3nm [50], though the electrochemical durability would be suffered due to the Gibbs-Thomson effect [27, 51, 52]. The atoms at corners and edges, with an increased prevalence at small particle size, are more susceptible to corrosion and dissolution. A number of possible explanations have been put forward to explain the particle size effect [17, 50, 53, 54] including surface defects, crystal phases, and particle shapes. The results from this work show that the synthesized Pt/C has slightly smaller particle size and higher ECA, but much pronounced decay rate in mass and specific activity than the TKK catalysts. This probably suggests that the one-step synthesis, relying primarily on surface adsorption and diffusion of adsorbates, may create a

more rough catalysts surface with less low-index crystal faces on the Pt particles. Though the rough (less ordered) surfaces could contribute to the ECA, the atoms at corners or edges will be easily lost, resulting in significant mass and specific activity losses. Future work is needed to understand the particle surface properties, i.e., wettability, defect density, and crystal structure, and to develop alloy catalysts.

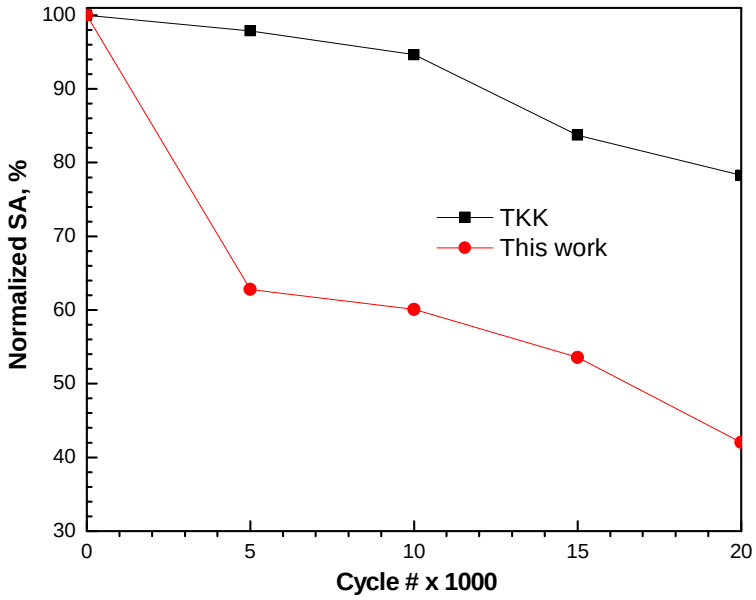

Figure 4.11 Decay of specific activity with time during potential cycles for the synthesized and TKK Pt/C catalysts. The initial area specific activities are 109.9 and 139.9 $\mu A/cm^2$ for the TKK and synthesized Pt/C catalysts, respectively.

4.2 Pt_3Co/C Catalysts

4.2.1 XRD Images

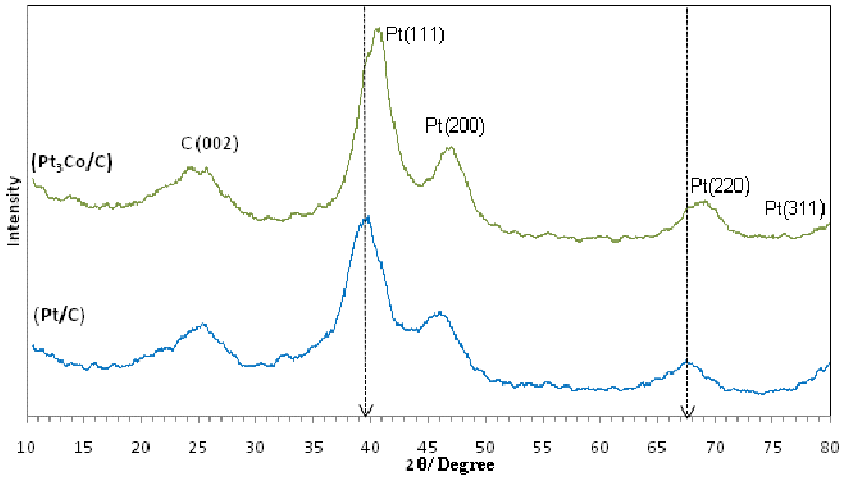

Figure 4.12 XRD Images of the Pt-based catalysts

From the diffraction peaks of Pt-alloy (Figure 4.12), we can note that the typical peaks corresponding to cobalt are not detected. However, it was found that the diffraction peak corresponding to Pt (111) showed a slight shift to a higher Bragg's angle (~1˚). This shift corresponds to a decrease in the lattice constant in the presence of the transitional metal (Co).This accounts for the formation of Pt-alloy in the catalyst [47] compared to that of Pt/C, indicating a lattice contraction arising from the substitution of the smaller Co atoms for the larger Pt atoms [55]. Also no individual cobalt peak was detected, which means cobalt might have alloyed with Pt crystal to form a disordered phase structure above the critical temperature of ~825℃ (Figure 4.13).

Table 4.4 Particle size of Pt-alloy nanoparticles

Catalyst	Particle size, nm
Pt	2.66
Pt-Co	3.97

The Pt-Co particle size was calculated using Scherrer' equation and shown in Table 4.4. The calculation indicates an increase in particle size of Pt_3Co/C at ~4.0nm when compared to Pt/C; this increase in particle size is attributed to the high temperature employed in the annealing process.

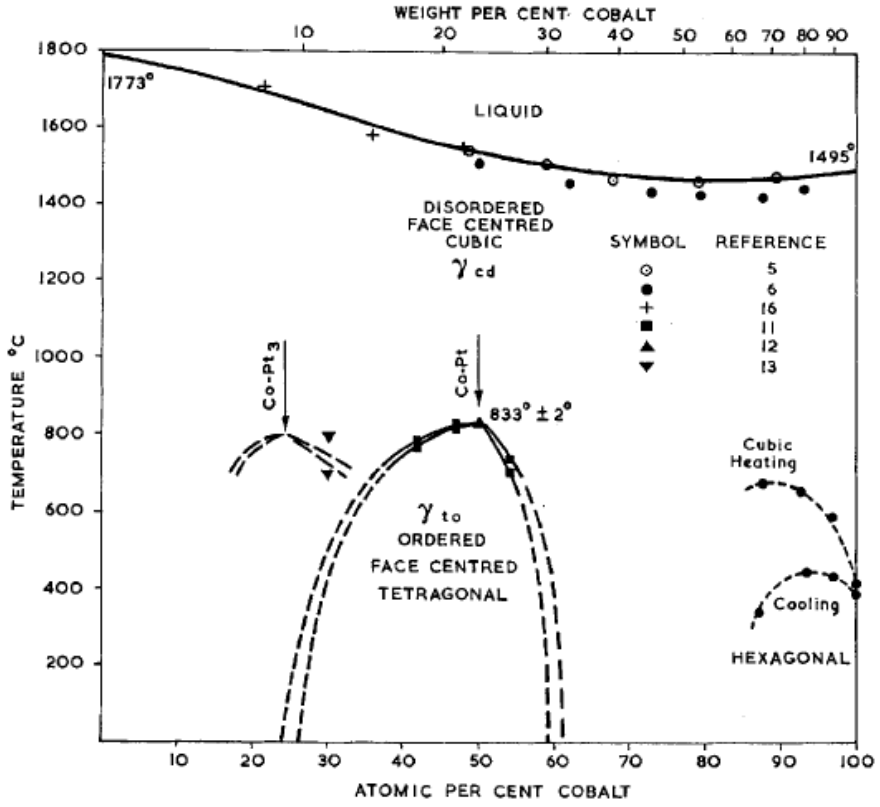

Figure 4.13 Equilibrium Diagram of Cobalt-Platinum systems [57].

In a review it was concluded that at a temperature range of about 500℃- 800℃ cobalt platinum in an atomic ratio of about 1:3 forms ordered structures. However at temperatures higher than critical

temperature ~825℃, platinum cobalt alloys form short range order. This type of disordered structure formation is presumed during alloy formation, as the temperature used for annealing platinum-cobalt catalyst was ~900℃ [57].

4.2.2 EDX Images

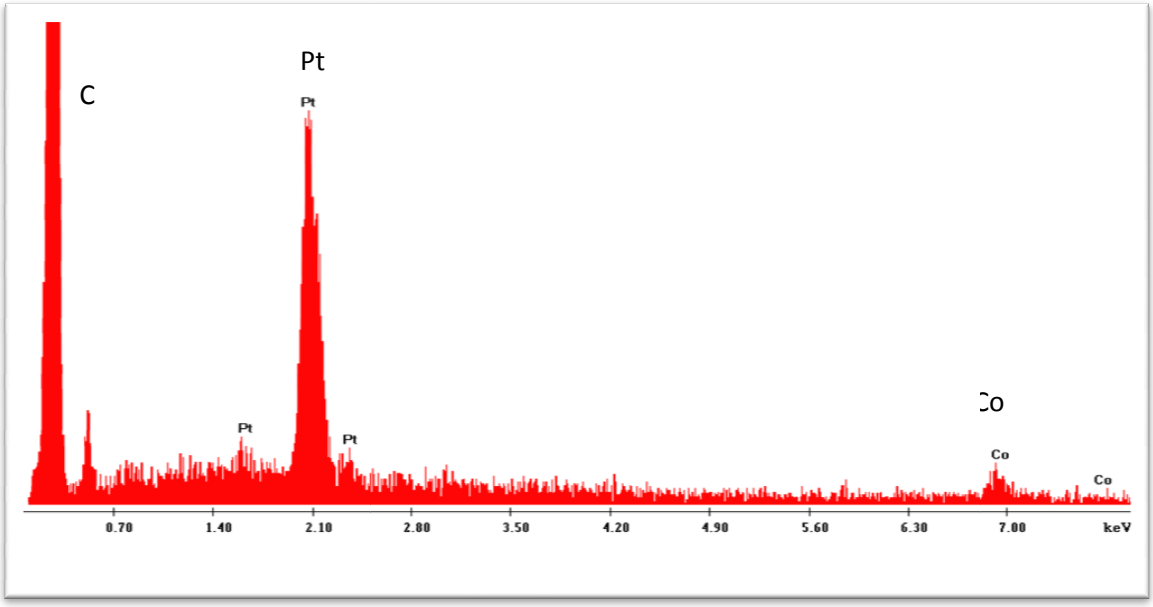

Figure 4.14 EDX Image for Pt-alloy catalyst

The presence of cobalt was confirmed through the EDX measurement obtained for Pt-alloy catalyst. The results are tabulated in Table 4.5.

Table 4.5 Pt and Co content in Pt_3Co/C catalyst

	Pt%	Co%
Pt_3Co/C	18	2

4.2.3 ECA and Activity

A cathodic shift of the onset of oxide formation is usually observed for alloyed Pt catalysts. The positive shift indicates the creation of weakly adsorbed oxide layer on the Pt surface, which is easier to reduce and therefore increases the ORR activity of the Pt-alloy [47]. However, in this study though suppression in Pt oxide formation is observed for the synthesized Pt_3Co catalyst (Figure 4.15), the peaks in CV curves are relatively flat. Therefore, it is suspected that the inhibition of oxide formation may be mainly due to larger particle size, rather than alloying.

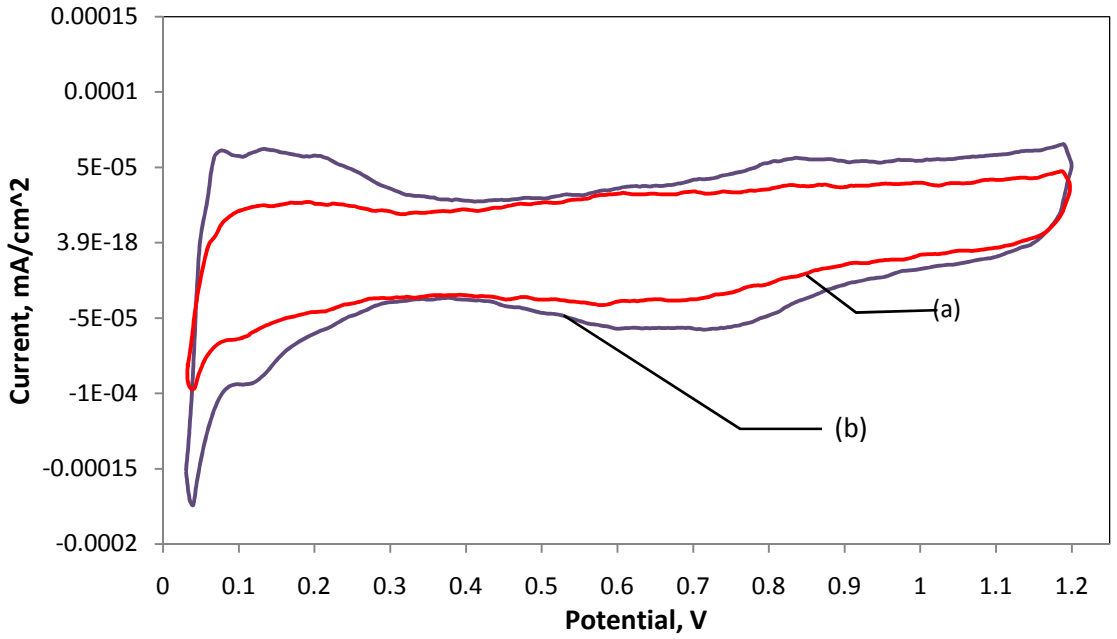

Figure 4.15 ECA values of a) Pt_3Co/C & c) Pt/C

The hydrogen adsorption and desorption potential in the region between 0.05 and 0.25 V versus SHE is similar for both Pt and Pt-alloys. However a reduction in the area attributed to adsorption and desorption of hydrogen was observed in the case of Pt alloys. This can be attributed to the increase in the particle size. The ECA values of the Pt-alloy and Pt/Cs is given in table 4.6.

Table 4.6 ECA Value of Pt-based catalysts

Samples	ECA (m^2/g)	
	Adsorption	Desorption
Pt/C	87.3	62.1
Pt_3Co/C	35.35	10.44

4.2.4 ORR Activity

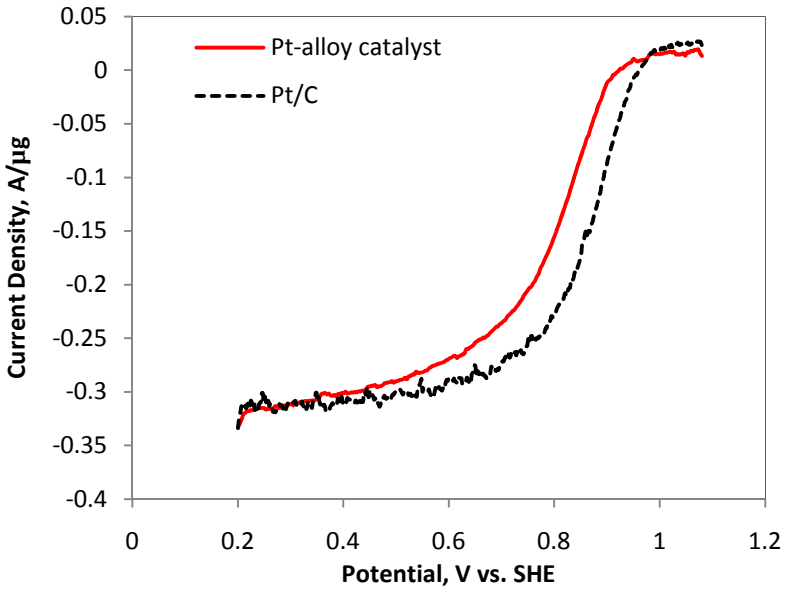

Figure 4.16 Polarization curves for Pt and Pt alloy catalysts on rotating disk electrode in 0.1M $HClO_4$ saturated with O_2 at room temperature and rotating speed of 1600rpm. The catalyst surface consists of a Pt loading of 2.7µg and about 0.5% by volume of Nafion in the Pt catalyst ink.

Figure 4.16 shows a typical polarization curve of 20% Pt/C and 20%Pt_3Co/C obtained at room temperature and in 0.1M$HClO_4$ saturated with O_2. The glassy carbon rotating disk electrode was rotated at 1600rpm. This region between 0.55 and 0.1 V versus SHE is purely the diffusion-limited region. At higher potentials, e.g., 0.8~0.9V, where the ORR is dominantly kinetics-controlled, the current generated from the alloy catalyst is only ~1/3 of that of Pt catalyst.

Catalyst activity has been shown strong correlation to factors such as the alloying element, platinum to metal (Pt/M) atomic ratio [27] and also particle size. Wu Bi *et al*. [27] have successfully demonstrated

alloying of cobalt with platinum in the atomic ration 3:1, enhanced the catalytic activity compared to 20%Pt/C ,and also reduced the Pt dissolution rate, thereby increasing the catalyst durability. However, in an attempt to obtain a higher catalyst activity in this study, the mass and specific activity of the Pt-alloy catalyst (Pt to Co in the ratio 3:1) decrease by a factor of ~2 and ~4 compared to those of the Pt/C. The mass and specific activity obtained for Pt-alloy catalyst and Pt are compared in table 4.7. Clearly, a correlation between catalyst activity and available electrochemical surface area might be the reason for the decreased activities. As from the XRD images, the particle sizes for Pt-alloy was found to be almost twice the size of Pt which can account for the reduced electrochemical surface area.

Table 4.7 Catalyst activity (mass activity and specific activity) of Pt3Co/C & Pt/C

Samples	$i_{m,}$ mA/µg	$i_{s,}$A/µcm^2
Pt/C	0.12	137.85
Pt_3Co/C	0.031	88.33

CHAPTER 5

CONCLUSION

The thesis focused on synthesis and detailed material/electrochemical characterization of two Pt-based catalysts, synthesized through a technique known as one-step synthesis. The method was designed to optimize the particle size and improve the overall Pt distribution in the catalyst, potentially resulting in both high active surface area and ORR activity. The Pt/C catalyst was compared to the commercial TKK Pt/C catalyst as well as to the Pt-alloy catalyst. Parameters including particle size, size distribution, ECA and ORR activity, and electrochemical durability were evaluated. It was found that the synthesized catalyst has slightly smaller particle size and narrow size distribution. The CV tests confirmed that the initial ECA for the synthesized sample was 30% higher than that of the TKK catalysts. Though the synthesized Pt/C showed higher ECA even after 20k potential cycles, however, its ECA decay rate is higher, especially from 5k to 20 k cycles. Studies on ORR activities indicated a faster decay in both mass and specific activities for the synthesized Pt/C than the TKK catalyst. Rough (less ordered) surfaces may contribute to such significant ECA and activity losses, as well as high initial ECA of the synthesized catalysts.

The ORR measurements for Pt-Co catalyst compared to Pt/C showed a decrease in ORR activity. From the experimental data it was concluded that this decrease in the mass and specific activities was due to the increase in particle size during the post annealing at high temperature. Although Pt-alloy catalysts show lower initial ECA activity, previous studies have proved that Pt alloy catalyst have lower decay rate when compared to Pt catalyst due to greater amounts of cobalt dissolution as compared to platinum [56].

The one-step synthesis proves to be a promising technique to obtain highly dispersed catalyst (Pt/C and Pt-alloy catalysts), active and highly durable fuel cell catalysts while lowering the cost of production.

Further investigation into platinum based binary and ternary catalysts can be conducted by using the above mentioned synthesis technique in order to overcome the inhibitive cost of platinum as a catalyst material in PEMFCs. Future work is needed to understand the particle surface properties, i.e., wettability, defect density, and crystal structure, and to control particle size of alloy catalysts.

REFERENCES

[1] R. L. Borup, J. R. Davey, F. H. Garzon, D. L. Wood, and M. A. Inbody, "PEM fuel cell electrocatalyst durability measurements," *Journal of Power Sources*, vol. 163, pp. 76-81, 2006.

[2] A. V. D. Rosa, *Fundamentals of Renewable Energy Sources*, 2 ed. London: Elsevier Inc., 2009.

[3] U. S. D. o. E.-E. E. a. R. Energy, "Type of Fuel Cells," 2011.

[4] J. Maier, "Nanoionics: ion transport and electrochemical storage in confined systems," *Nat Mater*, vol. 4, pp. 805-815, 2005.

[5] N. Rajalakshmi and K. S. Dhathathreyan, "Catalyst layer in PEMFC electrodes--Fabrication, characterisation and analysis," *Chemical Engineering Journal*, vol. 129, pp. 31-40, 2007.

[6] N. Sammes, *Fuel Cell Technology: Reaching Towards Commercialization*. London: Springer-Verlag, 2006.

[7] R. M. Rao, T. Oh, R. Rengaswamy, and W. M. a. C. Pantelides, "Scope for process systems engineering studies in proton exchange membrane fuel cells (PEMFC): A review of opportunities," in *Computer Aided Chemical Engineering*, vol. Volume 21: Elsevier, 2006, pp. 835-840.

[8] L. Xiong and A. Manthiram, "High performance membrane-electrode assemblies with ultra-low Pt loading for proton exchange membrane fuel cells," *Electrochimica Acta*, vol. 50, pp. 3200-3204, 2005.

[9] M. Prasanna, E. A. Cho, H. J. Kim, I. H. Oh, T. H. Lim, and S. A. Hong, "Performance of proton-exchange membrane fuel cells using the catalyst-gradient electrode technique," *Journal of Power Sources*, vol. 166, pp. 53-58, 2007.

[10] H. Kim, N. P. Subramanian, and B. N. Popov, "Preparation of PEM fuel cell electrodes using pulse electrodeposition," *Journal of Power Sources*, vol. 138, pp. 14-24, 2004.

[11] R. Benítez, J. Soler, and L. Daza, "Novel method for preparation of PEMFC electrodes by the electrospray technique," *Journal of Power Sources*, vol. 151, pp. 108-113, 2005.

[12] A. Bayrakçeken, A. Smirnova, U. Kitkamthorn, M. Aindow, L. Türker, I. Eroglu, and C. Erkey, "Pt-based electrocatalysts for polymer electrolyte membrane fuel cells prepared by supercritical deposition technique," *Journal of Power Sources*, vol. 179, pp. 532-540, 2008.

[13] X. Sun, R. Li, D. Villers, J. P. Dodelet, and S. Désilets, "Composite electrodes made of Pt nanoparticles deposited on carbon nanotubes grown on fuel cell backings," *Chemical Physics Letters*, vol. 379, pp. 99-104, 2003.

[14] J. Zhang, X. Wang, C. Wu, H. Wang, B. Yi, and H. Zhang, "Preparation and characterization of Pt/C catalysts for PEMFC cathode: effect of different reduction methods," *Reaction Kinetics and Catalysis Letters*, vol. 83, pp. 229-236, 2004.

[15] M. J. Escudero, E. Hontañón, S. Schwartz, M. Boutonnet, and L. Daza, "Development and performance characterisation of new electrocatalysts for PEMFC," *Journal of Power Sources*, vol. 106, pp. 206-214, 2002.

[16] Y. Shao, G. Yin, J. Wang, Y. Gao, and P. Shi, "Multi-walled carbon nanotubes based Pt electrodes prepared with in situ ion exchange method for oxygen reduction," *Journal of Power Sources*, vol. 161, pp. 47-53, 2006.

[17] M. Watanabe, H. Sei, and P. Stonehart, "The influence of platinum crystallite size on the electroreduction of oxygen," *Journal of Electroanalytical Chemistry and Interfacial Electrochemistry*, vol. 261, pp. 375-387, 1989.

[18] J. N. Soderberg, A. H. C. Sirk, S. A. Campbell, and V. I. Birss, "Oxygen reduction by sol-derived Pt/Co-based alloys for PEM fuel cells," *Journal of the Electrochemical Society*, vol. 152, pp. A2017-A2022, 2005.

[19] F. Liu and C.-Y. Wang, "Optimization of cathode catalyst layer for direct methanol fuel cells: Part I. Experimental investigation," *Electrochimica Acta*, vol. 52, pp. 1417-1425, 2006.

[20] R. S. Ingram and R. W. Murray, "Electroactive three-dimensional monolayers: Anthraquinone omega-functionalized alkanethiolate-stabilized gold clusters," *Langmuir*, vol. 14, pp. 4115-4121, 1998.

[21] J. Luo, M. M. Maye, N. N. Kariuki, L. Y. Wang, P. Njoki, Y. Lin, M. Schadt, H. R. Naslund, and C. J. Zhong, "Electrocatalytic oxidation of methanol: carbon-supported gold-platinum nanoparticle catalysts prepared by two-phase protocol," *Catalysis Today*, vol. 99, pp. 291-297, 2005.

[22] J. Luo, L. Y. Wang, D. Mott, P. N. Njoki, N. Kariuki, C. J. Zhong, and T. He, "Ternary alloy nanoparticles with controllable sizes and composition and electrocatalytic activity," *Journal of Materials Chemistry*, vol. 16, pp. 1665-1673, 2006.

[23] A. F. Gulla, M. S. Saha, R. J. Allen, and S. Mukerjee, "Dual Ion-Beam-Assisted Deposition as a Method to Obtain Low Loading-High Performance Electrodes for PEMFCs," *Electrochemical and Solid-State Letters*, vol. 8, pp. A504-A508, 2005.

[24] N. Cunningham, E. Irissou, M. Lefevre, M. C. Denis, D. Guay, and J. P. Dodelet, "PEMFC Anode with Very Low Pt Loadings Using Pulsed Laser Deposition," *Electrochemical and Solid-State Letters*, vol. 6, pp. A125-A128, 2003.

[25] S. Sambandam, V. Valluri, W. Chanmanee, N. de Tacconi, W. Wampler, W.-Y. Lin, T. Carlson, V. Ramani, and K. Rajeshwar, "Platinum-carbon black-titanium dioxide nanocomposite electrocatalysts for fuel cell applications," *Journal of Chemical Sciences*, vol. 121, pp. 655-664, 2009.

[26] J. Zhang, *PEM Fuel Cell Electrocatalysts and Catalyst Layers: Fundamentals and Applications*: Springer, 2008.

[27] W. Bi and T. F. Fuller, "Modeling of PEM fuel cell Pt/C catalyst degradation," *Journal of Power Sources*, vol. 178, pp. 188-196, 2008.

[28] S. M. a. S. Srinivasan, *The oxygen reduction/evolution reaction*, vol. 5 Part 5. United Kingdom: Wiley & Sons, 2009.

[29] H. A. Gasteiger, S. S. Kocha, B. Sompalli, and F. T. Wagner, "Activity benchmarks and requirements for Pt, Pt-alloy, and non-Pt oxygen reduction catalysts for PEMFCs," *Applied Catalysis B: Environmental*, vol. 56, pp. 9-35, 2005.

[30] M.-k. Min, J. Cho, K. Cho, and H. Kim, "Particle size and alloying effects of Pt-based alloy catalysts for fuel cell applications," *Electrochimica Acta*, vol. 45, pp. 4211-4217, 2000.

[31] P. N. R. Jr., "New Electrocatalysts for Fuel Cells," Lawrence Berkeley National Laboratory 2000.

[32] T. J. Schmidt, H. A. Gasteiger, G. D. Stab, P. M. Urban, D. M. Kolb, and R. J. Behm, "Characterization of High-Surface-Area Electrocatalysts Using a Rotating Disk Electrode Configuration," *Journal of The Electrochemical Society*, vol. 145, pp. 2354-2358, 1998.

[33] E. Higuchi, H. Uchida, and M. Watanabe, "Effect of loading level in platinum-dispersed carbon black electrocatalysts on oxygen reduction activity evaluated by rotating disk electrode," *Journal of Electroanalytical Chemistry*, vol. 583, pp. 69-76, 2005.

[34] A. Smirnova, X. Dong, H. Hara, A. Vasiliev, and N. Sammes, "Novel carbon aerogel-supported catalysts for PEM fuel cell application," *International Journal of Hydrogen Energy*, vol. 30, pp. 149-158, 2005.

[35] H. A. Gasteiger, J. E. Panels, and S. G. Yan, "Dependence of PEM fuel cell performance on catalyst loading," *Journal of Power Sources*, vol. 127, pp. 162-171, 2004.

[36] S. Srinivasan, F. J. Luczak, and S. Sarangapani, "EXPERIMENTAL METHODS IN LOW TEMPERATURE FUEL CELLS," in *Fuel Cells*: Springer US, 2006, pp. 267-308.

[37] V. Rai, "Experimental Investigation and Multi-scale Modeling of Polymer Electrolyte Fuel Cells," F. W. Venkat Viswanathan, Stephen Walch and Seung Hyun Kim, Ed. Stanford, 2006.

[38] C. D. Saquing, D. Kang, M. Aindow, and C. Erkey, "Investigation of the supercritical deposition of platinum nanoparticles into carbon aerogels," *Microporous and Mesoporous Materials*, vol. 80, pp. 11-23, 2005.

[39] B. Cangül, L. C. Zhang, M. Aindow, and C. Erkey, "Preparation of carbon black supported Pd, Pt and Pd-Pt nanoparticles using supercritical CO2 deposition," *The Journal of Supercritical Fluids*, vol. 50, pp. 82-90, 2009.

[40] N. T. Xuyen, H. K. Jeong, G. Kim, K. P. So, K. H. An, and Y. H. Lee, "Hydrolysis-induced immobilization of Pt(acac)2 on polyimide-based carbon nanofiber mat and formation of Pt nanoparticles," *Journal of Materials Chemistry*, vol. 19, pp. 1283-1288, 2009.

[41] O. A. Baturina, S. R. Aubuchon, and K. J. Wynne, "Thermal Stability in Air of Pt/C Catalysts and PEM Fuel Cell Catalyst Layers," *Chemistry of Materials*, vol. 18, pp. 1498-1504, 2006.

[42] R. V. Krishnarao, "Formation of SiC whiskers from rice husk silica-carbon black mixture: effect of preheat treatment," *Journal of Materials Science Letters*, vol. 12, pp. 1268-1271, 1993.

[43] D. J. Zhao, G. P. Yin, and J. Wei, "Non-Platinum Cathode Electrocatalysts in Polymer Electrolyte Membrane Fuel Cells," *Progress in Chemistry*, vol. 21, pp. 2753-2759, 2009.

[44] J. Wang, G. Yin, Y. Shao, S. Zhang, Z. Wang, and Y. Gao, "Effect of carbon black support corrosion on the durability of Pt/C catalyst," *Journal of Power Sources*, vol. 171, pp. 331-339, 2007.

[45] L. M. Roen, C. H. Paik, and T. D. Jarvi, "Electrocatalytic Corrosion of Carbon Support in PEMFC Cathodes," *Electrochemical and Solid-State Letters*, vol. 7, pp. A19-A22, 2004.

[46] K. Kinoshita, *Carbon*: Wiley, New York 1988.

[47] H. R. Colón-Mercado and B. N. Popov, "Stability of platinum based alloy cathode catalysts in PEM fuel cells," *Journal of Power Sources*, vol. 155, pp. 253-263, 2006.

[48] T. J. S. a. H. A. Gasteiger, *Rotating thin-film method for supported catalysts*, vol. 2: Wiley, 2003.

[49] *S. Mukerjee and S. Srinivasan, in: W. Vielstich, H. Gasteiger, A. Lamm (Eds.), Handbook of Fuel Cells: Fundamentals, Technology and Applications, vol. 3, John Wiley & Sons, Ltd., 2003.*

[50] K. Kinoshita, "Particle Size Effects for Oxygen Reduction on Highly Dispersed Platinum in Acid Electrolytes," *Journal of The Electrochemical Society*, vol. 137, pp. 845-848, 1990.

[51] R. M. Darling and J. P. Meyers, "Mathematical Model of Platinum Movement in PEM Fuel Cells," *Journal of The Electrochemical Society*, vol. 152, pp. A242-A247, 2005.

[52] W. Bi and T. F. Fuller, "Temperature Effects on PEM Fuel Cells Pt/C Catalyst Degradation," *Journal of The Electrochemical Society*, vol. 155, pp. B215-B221, 2008.

[53] L. J. Bregoli, "The influence of platinum crystallite size on the electrochemical reduction of oxygen in phosphoric acid," *Electrochimica Acta*, vol. 23, pp. 489-492, 1978.

[54] Y. Takasu, N. Ohashi, X. G. Zhang, Y. Murakami, H. Minagawa, S. Sato, and K. Yahikozawa, "Size effects of platinum particles on the electroreduction of oxygen," *Electrochimica Acta*, vol. 41, pp. 2595-2600, 1996.

[55] L. Xiong and A. Manthiram, "Influence of atomic ordering on the electrocatalytic activity of Pt-Co alloys in alkaline electrolyte and proton exchange membrane fuel cells," *Journal of Materials Chemistry*, vol. 14, pp. 1454-1460, 2004.

[56] P. Yu, M. Pemberton, and P. Plasse, "PtCo/C cathode catalyst for improved durability in PEMFCs," *Journal of Power Sources*, vol. 144, pp. 11-20, 2005

[57] A.S. Darling, "Cobalt-Platinum Alloys- A critical review of their constitution and Properties", *Platinum Metals Rev.,* 1963, **7,** (3)96-104.

BIOGRAPHICAL INFORMATION

Sonam Patel lived in Bangalore, India. In 2007 she completed her bachelor in engineering from the Department of Chemical Engineering at M.S. Ramaiah Institute of Technology, Bangalore, India.

In the same year she joined the National Aerospace Laboratories, (NAL) Bangalore, India as a Project Trainee in the Experimental Aerodynamics Division of NAL. In order to pursue higher education she joined the Department of Materials Science and Engineering at the University of Texas, Arlington (UTA), TX in 2008 to pursue her Masters' Degree. After a short stint at the Department of Biomedical Engineering on a project related to Temperature Sensitive Composite Hydrogels for Drug Delivery, in the Tissue engineering laboratory, she worked as a research assistant for one year at the Electrochemical Laboratory, UTA.

Her area of research covered synthesis and characterization studies on Pt and Pt-based catalysts for hydrogen fuel cells. After the completion of her masters' degree, she will be looking for a full time research oriented position in the area of nano-materials.